

Pulsed laser deposition of single phase n- and p-type Cu₂O thin films with low resistivity

Syed Farid Uddin Farhad^{1, 2, 3, 4*}, David Cherns¹, James Smith², Neil Fox^{1, 2}, and David Fermín³

¹H.H. Wills Physics Laboratory, School of Physics, University of Bristol, BS8 1TL, UK

²Diamond Laboratory, School of Chemistry, University of Bristol, BS8 1TS, UK

³Electrochemistry Laboratory, School of Chemistry, University of Bristol, BS8 1TS, UK

⁴Industrial Physics Division, BCSIR Laboratories, Dhaka, Bangladesh Council of Scientific and Industrial Research (BCSIR), Dhaka 1205, Bangladesh

*Corresponding Author: sf1878@my.bristol.ac.uk , s.f.u.farhad@bcsir.gov.bd

Abstract

Low resistivity ($\rho \sim 3\text{-}24 \text{ m}\Omega\cdot\text{cm}$) with tunable n- and p-type single phase Cu₂O thin films have been grown by pulsed laser deposition at 25-200 °C by varying the background oxygen partial pressure (O_{2pp}). Capacitance data obtained by electrochemical impedance spectroscopy was used to determine the conductivity (n- or p-type), carrier density, and flat band potentials for samples grown on indium tin oxide (ITO) at 25 °C. The Hall mobility (μ_H) of the n- and p-type Cu₂O was estimated to be $\sim 0.85 \text{ cm}^2\cdot\text{V}^{-1}\text{s}^{-1}$ and $\sim 4.78 \text{ cm}^2\cdot\text{V}^{-1}\text{s}^{-1}$ respectively for samples grown on quartz substrate at 25 °C. An elevated substrate temperature $\sim 200 \text{ }^\circ\text{C}$ with $O_{2pp} = 2 - 3 \text{ mTorr}$ yielded p-type Cu₂O films with six orders of magnitude higher resistivities in the range, $\rho \sim 9 - 49 \text{ k}\Omega\cdot\text{cm}$ and mobilities in the range, $\mu_H \sim 13.5 - 22.2 \text{ cm}^2\cdot\text{V}^{-1}\text{s}^{-1}$. UV-Vis-NIR diffuse reflectance spectroscopy showed optical bandgaps of Cu₂O films in the range of 1.76 to 2.15 eV depending on O_{2pp} . Thin films grown at oxygen rich conditions $O_{2pp} \geq 7 \text{ mTorr}$ yielded mixed phase copper oxide irrespective of the substrate temperatures and upon air annealing at 550 °C for 1 hour completely converted to CuO phase with n-type semiconducting properties ($\rho \sim 12 \text{ }\Omega\cdot\text{cm}$, $\mu_H \sim 1.50 \text{ cm}^2\text{V}^{-1}\text{s}^{-1}$). The as-grown p- and n-type Cu₂O showed rectification and a photovoltaic response in solid junctions with n-ZnO and p-Si electrodes respectively. Our findings may create new opportunities for devising Cu₂O based junctions requiring low process temperatures.

Keywords: Pulsed Laser Deposition; Cuprous oxide (Cu₂O) thin film; p- and n-type conductivity; Hall coefficient measurement; Fermi level; Mott-Schottky analyses.

1. Introduction

The semiconductor cuprous oxide (Cu_2O), has shown much promise in photocatalytic water splitting [1], resistive switching devices [2], thin film transistors (TFT) [3], gas sensors [4], as an anode material in Li-ion based batteries [5] and in photovoltaic (PV) applications [6]. It is non-toxic, Earth-abundant, and could be prepared by physical and chemical methods [6-8]. In addition, single phase Cu_2O is desirable as an absorber material for solar cells because of its reported direct bandgap ($E_g \sim 2.17$ eV) and high absorption coefficient (above 10^5 cm^{-1}) in the visible region of solar radiation and, potentially, the ability to dope both n- and p-type via manipulating processing conditions [9-15]. The natural p-type conductivity of Cu_2O is believed to stem from copper vacancies (V_{Cu}) in the crystal lattice [16, 17], and its suitable band alignment with other wide bandgap n-type metal oxide semiconductors, such as ZnO [18, 19] and TiO_2 [20, 21], makes it attractive for realizing reasonably efficient heterojunction solar cells. In contrast, the origin of intrinsic n-type conductivity is a matter of debate [9, 22, 23], yet it has gained substantial interest because of the possibility of the formation of homojunction solar cells [7, 9, 12, 14, 24] to suppress the deleterious interfacial defects states often formed in the case of most heterojunction solar cells ([25] and refs. therein). The oxygen vacancy (V_{O}) [11] and copper interstitial (Cu_i) defects in Cu_2O lattice have been proposed for the electron-donating source in explaining the experimental results ([22] and refs. therein). However, the formation energy of V_{O} is relatively low compared to that of Cu_i irrespective of the copper-rich (poor)/oxygen-poor (rich) growth conditions [22]. In general, the donor- and acceptor- levels should be shallow for effective n- and p- type semiconductors. Carrier concentrations over of $\sim 10^{16} \text{ cm}^{-3}$ and mobilities at least $\sim 5 \text{ cm}^2/\text{V.s}$ are also necessary for efficient Cu_2O based optoelectronic devices [11, 26, 27]. In the case of intrinsic n-type Cu_2O , most of the experimental works reported deep donor levels ([22] and refs. therein), therefore, unlikely to overcome the native p-type conductivity stemming from cation deficiency (V_{Cu}) [6] due to self-compensation [28]. However, a recent report by Nandy et al. demonstrated that controlling the oxygen vacancies (V_{O}) into the Cu_2O crystal (i.e., $\text{Cu}_2\text{O}_{1-\delta}$) may induce an impurity state close to the conduction band thereby enhancing the electron-donating ability due to the unshared d-electrons of Cu atoms (nearest to the vacancy site) [29]. Their theoretical approach further suggested that the formation energy for obtaining 2.08% ($\delta=0.208$) of V_{O} in Cu_2O could be as low as 0.32 eV under oxygen deficient condition, suggesting that the stable $\text{Cu}_2\text{O}_{1-\delta}$ entity maybe experimentally viable [29].

Several physical [6, 25, 30-32] and wet-chemical [3, 5, 15, 33-36] based deposition methods have been employed to produce phase pure Cu_2O . Among them, pulsed laser deposition (PLD) offers good control on a wide range of processing parameters such as laser wavelength, pulse repetition rate, laser energy per pulse (LP), background gas pressure ($\text{O}_{2\text{pp}}$), substrate temperature (T_{sub}) etc. and has been demonstrated to give single phase cuprous oxides with good structural, morphological and electrical properties [11, 25, 27, 37, 38]. Previous work [25, 37] demonstrated the similar microstructures of Cu_xO_y (a defect variant of the basic- Cu_2O) thin films on various substrates using different PLD processing conditions, these identified favorable process conditions within which we now focus. These investigations, on the effect of $T_{\text{sub}} (\leq 400^\circ\text{C})$ and $\text{O}_{2\text{pp}} (\leq 10 \text{ mTorr})$, achieve single phase Cu_2O with varying optical and electrical properties by exploiting the non-equilibrium deposition environment of PLD. The ablation species react with ambient background gas chemically and physically while it proceeds towards the substrate from the target and affects the resulting film properties. Oxygen content in copper oxide films can be adjusted through controlling the oxygen partial pressure ($\text{O}_{2\text{pp}}$) during growth. In the literature most of the investigations related to electrical properties of Cu-O films deal with films deposited under oxygen rich conditions near the $\text{Cu}_2\text{O}/\text{CuO}$ boundary. There is less information for films deposited at the $\text{Cu}/\text{Cu}_2\text{O}$ boundary, where an n-type Cu_2O may exist [39] due to the predominant presence of oxygen vacancy (V_{o}) as opposed to the hole creating copper vacancy (V_{cu}). Meyer et al. [6], roughly estimated the binding energy of donor and acceptors for Cu_2O to be 266 meV and 156 meV using effective mass theory (EMT) and discussed that carrier densities well above $\sim 10^{18} \text{ cm}^{-3}$ are necessary to overcome natural p-type conductivity due to the cation vacancy (V_{cu}). Wang et al. [40] argued that n-type conductivity of Cu_2O is possible only if the V_{o} would exist at very high concentrations synthesized in oxygen poor conditions. In our previous report we demonstrated the n-type conductivity of Cu_2O based on electrochemical Mott-Schottky analyses for the samples grown by PLD at room temperature with oxygen poor condition ($\text{O}_{2\text{pp}} \ll 1 \text{ mTorr}$) [41]. Recently, Xu et al. [11], also reported PLD grown phase pure Cu_2O films produced at 600°C under oxygen poor conditions ($\text{O}_{2\text{pp}} = 0.09 \text{ Pa} \approx 0.68 \text{ mTorr}$). The films exhibited p-type conductivity and upon post N_2 plasma treatment of the as-deposited samples they observed a phase transition from pure Cu_2O to a mixture of Cu_2O and Cu with an accompanied change from p to n-type conduction. Therefore, in this work, the effects of $\text{O}_{2\text{pp}}$ (both oxygen-rich and oxygen-poor conditions) in controlling composition, microstructure, optical, electrical, and electrochemical impedance properties of PLD Cu_2O films were investigated. We found that under suitable deposition

conditions both n- and p-type copper oxide thin films can be realized which are discussed below.

2. Experimental methods

2.1 Growth of PLD films

A simple PLD setup using a UV-ArF Excimer Laser (wavelength: 193 nm, repetition rate: 10 Hz, pulsed width: 20 ns, spot size: $\sim 1 \text{ mm}^2$, energy (LP): $25 \pm 4 \text{ mJ/pulse}$) was used to deposit copper oxide thin films on amorphous quartz, polycrystalline ITO, and single crystalline NaCl(100) substrates under the following conditions: Base vacuum of the PLD chamber $\leq 10^{-5} \text{ Torr}$; oxygen partial pressure ($\text{O}_{2\text{pp}}$): 0 – 10 mTorr; target-substrate distance $\sim 5 \text{ cm}$; substrate temperature (T_{sub}): ranging from non-intentionally heated ($\text{RT} \sim 25^\circ\text{C}$) – 400°C . The substrate temperature was controlled by halogen bulb heater and measured by using a digital thermocouple as described in ref. [25]. The substrate temperature and oxygen partial pressure were varied to allow the film to grow in a stable regime, where no decomposition of the film was observed. Post annealing treatment was also given to some of the as-grown Cu_2O films under controlled O_2 ambient inside the PLD chamber for comparison purposes.

Prior to film deposition, all substrates were ultrasonically cleaned successively in Toluene Acetone, isopropanol and ultra-pure water (Mili-Q, $18 \text{ M}\Omega\cdot\text{cm}$) for 15 min followed by a Ar blown dry. All substrates were subjected to an UV-Ozone clean for 20 min immediately before being mounted in the PLD chamber. The target material was commercially available hot pressed ceramic Cu_2O (purity $\sim 99.95\%$). The target was ablated for 5 min prior to actual deposition on the substrates.

2.2 Characterization of PLD samples

The X-ray Diffraction (XRD) spectra were recorded with Bruker AXS D8 Advance powder X-ray diffractometer using $\text{Cu K}\alpha$ ($\lambda = 1.5406 \text{ \AA}$) radiation. The diffraction patterns were recorded with a step size of $\sim 0.025^\circ$ and a time per step of 18 s, the samples were rotated to homogenize the measurements. TEM analyses of samples grown on NaCl(100) were investigated by a JEOL 2010 and a Philips EM 430 as described in ref. [25] where the TEM camera length calibration procedure was also discussed. Raman and Photoluminescence spectra were recorded at room temperature in the backscattering geometry with a Renishaw 2000 confocal spectrometer using $\lambda_{\text{ext}} = 514.5 \text{ nm}$ Ar-ion laser ($P \leq 5 \text{ mW}$) as an excitation source. The optical transmission and diffuse reflection measurements of films deposited on

quartz substrate were made using a UV-VIS-NIR spectrophotometer (Shimadzu UV2600 plus) coupled with an integrating sphere. Sheet resistance was measured by a Keithley 2400 source-measure-unit (SMU) coupled with a custom made collinear 4-point probe. Measurements of highly resistive films ($>200\text{ M}\Omega$) were carried out using a precision current source (Keithley 6221 AC/DC) coupled with a Nanovoltmeter (Keithley 2182A). To minimize the non-uniformity nature of the PLD thin film, measurements were performed over three or more different areas of the sample to get a final resistance value. Thicknesses of the PLD films were estimated by combined analyses of FE-SEM (JEOL JSM 6330F) cross-sectional imaging and Variable Angle Spectroscopic Ellipsometry (VASE) (M-2000 U, J.A. Woollam Co.) [37]. Hall mobilities of samples grown on quartz were measured as accurately as possible using a homemade Hall coefficient measurement setup utilizing a commercial 1 Tesla permanent magnet (Magnetsales UK Ltd.) with gold coated electrical contact pads in the van der Pauw sample configuration (see supplementary materials for details). Both Cyclic Voltammetry (CV) and Electrochemical Impedance Spectroscopy (EIS) measurements were performed under dark conditions using a Potentiostat (Autolab, PGSTAT-30) equipped with a frequency analyzer. An AC signal of 20 mV amplitude with frequencies ranging from 50 Hz to 10 kHz was applied at a set of constant bias voltage over a narrow potential window to preserve the stability of the Cu_2O film. The Keithley SMU coupled with a homemade multiprobe workstation was also used to measure I-V curve of the Cu_2O -based solid p-n junctions.

3. Results and discussion

Four sets of samples were deposited in an attempt to grow high quality single phase copper (I) oxide (Cu_2O) at relatively low temperatures with a range of conductivities. In the first two sets of samples, substrate temperature was varied from $25\text{ }^\circ\text{C}$ (RT) to $400\text{ }^\circ\text{C}$ with two different constant oxygen partial pressure ($\text{O}_{2\text{pp}}$), namely 3 mTorr and 10 mTorr , in order to find out the optimum process conditions for single phase copper oxide. In the other two sets, the oxygen content inside the PLD chamber was varied ($0 \leq \text{O}_{2\text{pp}} \leq 7\text{ mTorr}$) at two substrate temperatures (T_{sub}), $25\text{ }^\circ\text{C}$ and $200\text{ }^\circ\text{C}$. The PLD thin films grown at $25\text{ }^\circ\text{C} \leq T_{\text{sub}} \leq 400\text{ }^\circ\text{C}$ with constant $\text{O}_{2\text{pp}} \approx 10\text{ mTorr}$ were found to be mainly composed of a mixture of Cu_2O and more O-rich Cu-O phases as evident from the XRD analyses (see Fig. S1a for details). Therefore, the oxygen rich ($\text{O}_{2\text{pp}} = 10\text{ mTorr}$) samples will not be considered further

in the discussion below. As a quick guide for the readers: the structural, compositional, and electrical characteristics of samples investigated are summarized in Fig. 1.

The microstructure and surface morphology of Cu (I) oxide thin films are seemingly independent of substrate material as investigated by XRD and FE-SEM where all films are polycrystalline in nature showing grain sizes in the range 50 nm to 150 nm, but with some larger grains and texture on crystalline substrates (see Fig. S1.1 and Fig. S5.1 to S5.4 in supplementary material).

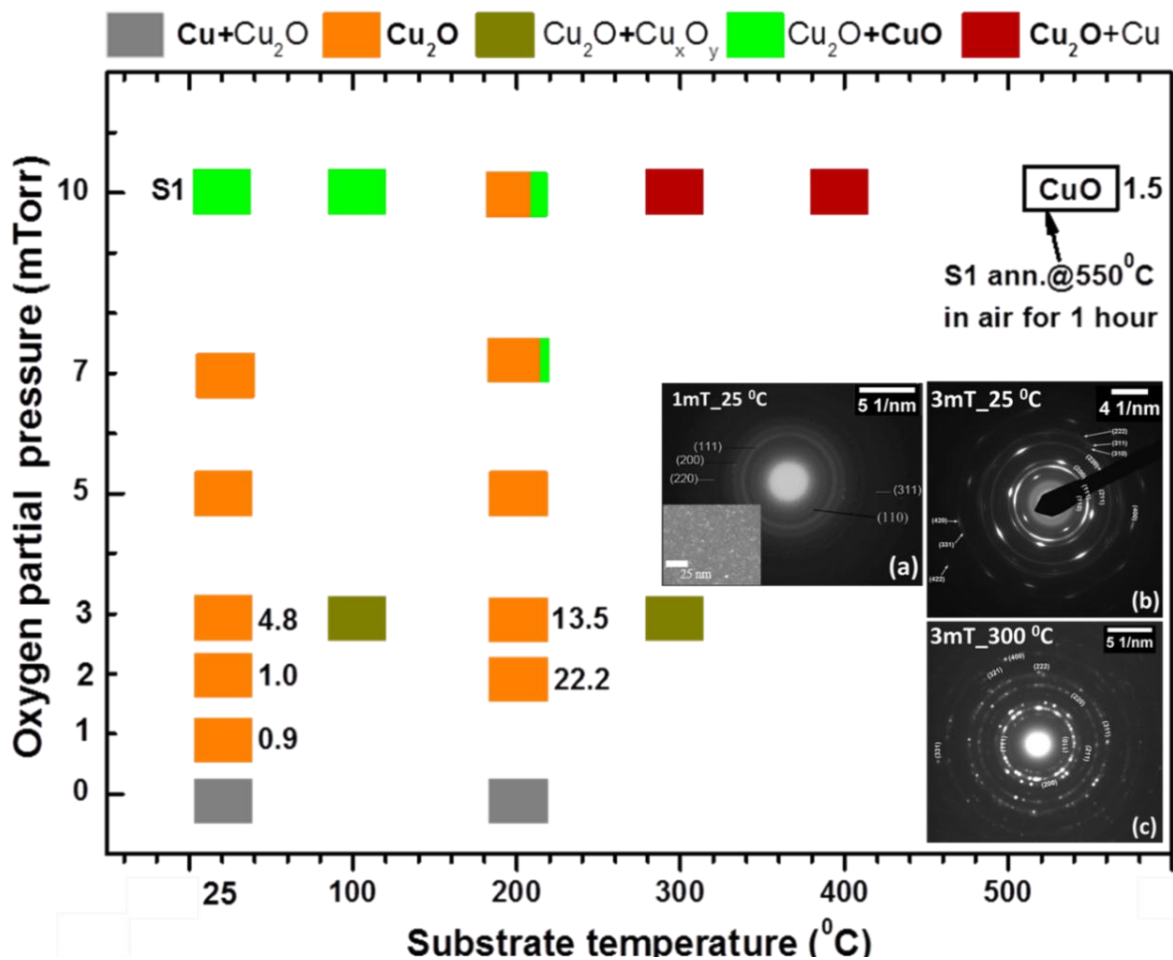


Fig. 1. (color online) Deposition diagram of PLD grown copper oxide phases with varying $\text{O}_{2\text{pp}}$ and T_{sub} . The colored squares represent the different phase compositions shown at the top of the graph. The carrier mobility of some as-deposited and annealed S1(Cu(II) oxide: CuO) films are also included in the analysis for comparison purposes. SAED patterns of samples grown on NaCl (100) with (a) $\text{O}_{2\text{pp}} = 1 \text{ mTorr}$, $T_{\text{sub}} = 25^{\circ}\text{C}$ (Inset: bright field image), (b) $\text{O}_{2\text{pp}} = 3 \text{ mTorr}$, $T_{\text{sub}} = 25^{\circ}\text{C}$, and (c) $\text{O}_{2\text{pp}} = 3 \text{ mTorr}$, $T_{\text{sub}} = 300^{\circ}\text{C}$ are showing single phase Cu(I) oxide with different morphologies.

It can be seen from Fig. 1 (Green, brown, and mixed colored squares) that elevated T_{sub} and high level $O_{2\text{pp}} \geq 7$ mTorr produced a mixture of Cu-O phases evident from XRD and Raman analyses (shown in Fig. S1-S2 in supplementary materials). In contrast, substrate temperature 100°C and 300°C with fixed $O_{2\text{pp}} = 3$ mTorr produce non-stoichiometric Cu (I) oxide ($\text{Cu}_2\text{O} + \text{Cu}_x\text{O}_y$) exhibiting cubic SAED patterns similar to phase pure polycrystalline Cu_2O (see also Fig. S1b). The origin of the Cu_xO_y phase - a defect structure of Cu_2O - was discussed in detail in our previous report [25]. It should be noted that depositing films at $T_{\text{sub}} = 25^\circ\text{C}$ and $T_{\text{sub}} = 200^\circ\text{C}$ while tuning the $O_{2\text{pp}}$ allows one to achieve single phase Cu_2O with varying electrical properties (see orange color squares and numerical value for carrier mobility in Fig. 1). The structural properties of these films are presented in Fig. 2 below.

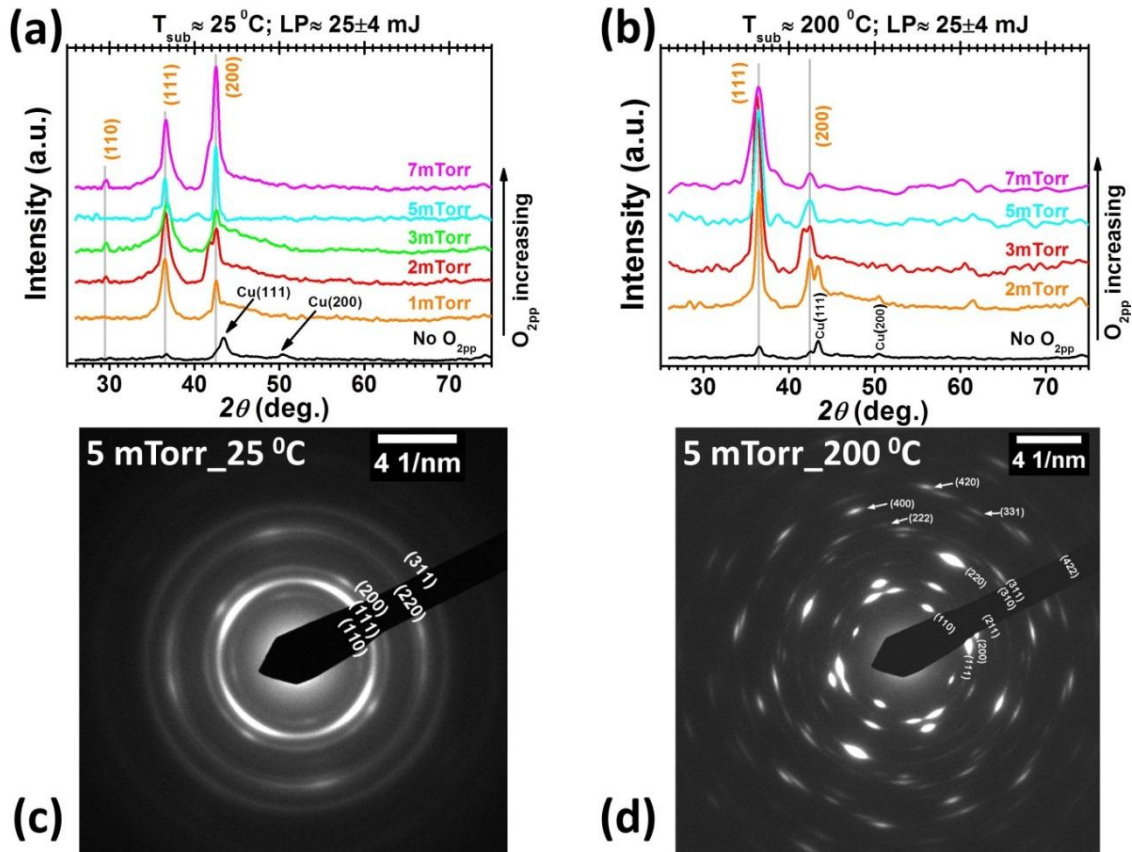


Fig. 2a and 2b show the XRD profiles of as-grown films deposited at $T_{\text{sub}} = 25^\circ\text{C}$ (RT-grown) and $T_{\text{sub}} = 200^\circ\text{C}$ (HT-grown), respectively, on quartz substrates with varying $O_{2\text{pp}}$. XRD results revealed that single phase Cu_2O , with no contribution from Cu and CuO, could be produced with $1 \text{ mTorr} \leq O_{2\text{pp}} \leq 7 \text{ mTorr}$ in the case of RT-grown and with $3 \text{ mTorr} \leq O_{2\text{pp}} \leq 5 \text{ mTorr}$ in the case of HT-grown thin films. In these phase purity limits, both RT- and HT-grown mainly exhibit $\text{Cu}_2\text{O}(111)$ and $\text{Cu}_2\text{O}(200)$ Bragg peaks but the former displays an additional $\text{Cu}_2\text{O}(110)$ peak at $2\theta \approx 29.5^\circ$. Metallic Cu inclusions were observed in the RT-grown film with $O_{2\text{pp}} < 1 \text{ mTorr}$ and in the HT-grown film with $O_{2\text{pp}} \leq 2 \text{ mTorr}$ presumably due to the deficiency of oxygen species in the PLD chamber. However, RT-grown film with $O_{2\text{pp}} = 1 \text{ mTorr}$ show single phase Cu_2O films evident from XRD and SAED pattern (see Fig. 2a and Fig. 1a). Both RT- and HT-grown films with $O_{2\text{pp}} > 7 \text{ mTorr}$ were found to be mixed Cu-O phase (see Fig. S2) with CuO as a major product. Notice also that RT- and HT-grown films approached towards strong $\{100\}$ and $\{111\}$ texturing, respectively, with increasing $O_{2\text{pp}}$ up to 7 mTorr (see also Fig. S3a). The average crystallite domain size estimated by using Scherrer formula was found to be in the range 5 – 15 nm and found to be following a decreasing trend with increasing $O_{2\text{pp}}$ (for details see fig. S3b) most probably due to the inclusion of oxygen rich Cu-O phase at higher $O_{2\text{pp}}$ [37]. However, up to $O_{2\text{pp}} = 5 \text{ mTorr}$, PLD grown thin films are composed of Cu(I) oxide as evident from the SAED patterns shown in Fig. 2c and 2d. The arced SAED patterns, more conspicuous in Fig. 2d, is due to the micro-twinning on $(\bar{1}1\bar{1})$, $(1\bar{1}\bar{1})$, $(1\bar{1}1)$ and $(11\bar{1})$ planes while viewed down the $[011]$ zone axis [25].

Room temperature Raman analyses have also been conducted to supplement the XRD results in order to further confirm the phase purity of RT-grown and at HT-grown samples deposited with $2 \text{ mTorr} \leq O_{2\text{pp}} \leq 7 \text{ mTorr}$ which are presented in Fig. 3 below. All Raman peaks in both groups of samples can be assigned with reported phonon modes of Cu_2O crystal only (solid lines) [25], except for the HT-grown with $O_{2\text{pp}} = 7 \text{ mTorr}$ film which is seen to be a mixture of Cu_2O (solid lines) and CuO (dotted lines) (cf. Fig. 3a and 3b). The presence of CuO phase is confirmed by the additional presence of A_g and $B_g^{(1)}$ modes at $\sim 296 \text{ cm}^{-1}$ and $\sim 346 \text{ cm}^{-1}$ respectively (see top panel in Fig. 3b). The position of Raman peaks for copper oxide compounds vary considerably in literature, but the vibrational modes for all three copper oxide phases cited in references [6, 25, 42] clearly indicate that none of the Raman signals in figure 3 (up to $O_{2\text{pp}} \approx 5 \text{ mTorr}$ in the case of HT-grown films) are related to CuO and/or Cu_4O_3 phases.

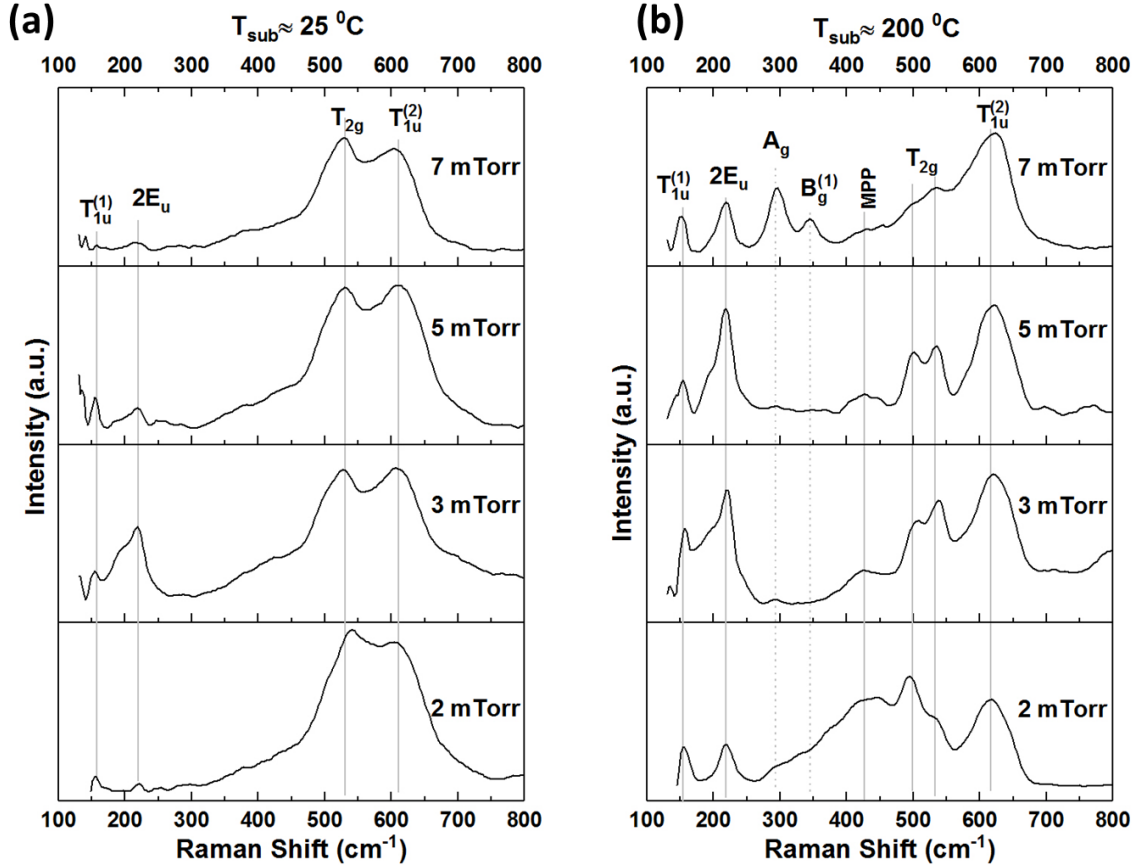


Fig. 3. Room temperature Raman spectra of, as-grown copper oxide thin films on quartz glass as a function of O_{2pp} at $T_{sub} \approx 25$ °C (a), and at $T_{sub} \approx 200$ °C (b). Vertical lines represent the reference vibrational mode of copper oxide.

The room temperature Photoluminescence (RT-PL) of thin films grown at $T_{sub} \approx 25$ °C(RT) and $T_{sub} \approx 200$ °C(HT) with $2 \text{ mTorr} \leq O_{2pp} \leq 5 \text{ mTorr}$ including Cu_2O PLD target are shown in Fig. 4. All luminescence peaks (solid lines) can be attributed to copper oxide phases, consistent with the results reported previously [25]. The exciton-related ($X_0 - \Gamma_{12}^-$) emission peak is clearly seen in the RT-PL spectrum for all PLD films including the target material suggesting good quality Cu_2O thin films irrespective of O_{2pp} conditions. The luminescence peaks centering at $\sim 760 \text{ nm}$ and $\sim 880 \text{ nm}$ have been put forward for Cu_3O_2 and $[V_{Cu}^- - V_O^+]$ complex respectively [25]. Notice that at low $O_{2pp} = 2 - 3 \text{ mTorr}$, HT-grown films showed an enhanced ($X_0 - \Gamma_{12}^-$) peak with additional $[V_{Cu}^- - V_O^+]$ complex peak which is not conspicuous in RT-grown films. These samples also exhibited diminished V_{cu} peak (see Fig. 4b).

The optical band gap thus approaches the bandgap value of bulk Cu_2O ($E_g = 2.17$ eV), and presumably therefore stoichiometric phase formation, at optimum values of $\text{O}_{2\text{pp}}$. The lowest measured optical bandgap (~ 1.65 eV) of HT-grown $\text{O}_{2\text{pp}} = 7$ mTorr film suggests an oxygen rich Cu-O phase as also evident from its Raman spectrum (see top panel in Fig. 3b). The RT-grown sample (S1) annealed in air at 550°C for 1 hour also exhibited a lower optical bandgap ~ 1.45 eV due to complete conversion to CuO (see Fig. S4 in supplementary material). The lower optical bandgap for films with low $\text{O}_{2\text{pp}}$, suggest oxygen vacancies (V_o) which introduce defect states in the bandgap leading to a lower effective bandgap compared to the stoichiometric Cu_2O .

Fig. 6 (below) shows the four point collinear probe measured electrical resistivity of RT- and HT-grown films as a function of $\text{O}_{2\text{pp}}$. The data points for the films grown without O_2 injection in the PLD chamber have also been included in the analyses for the sake of completeness and comparison.

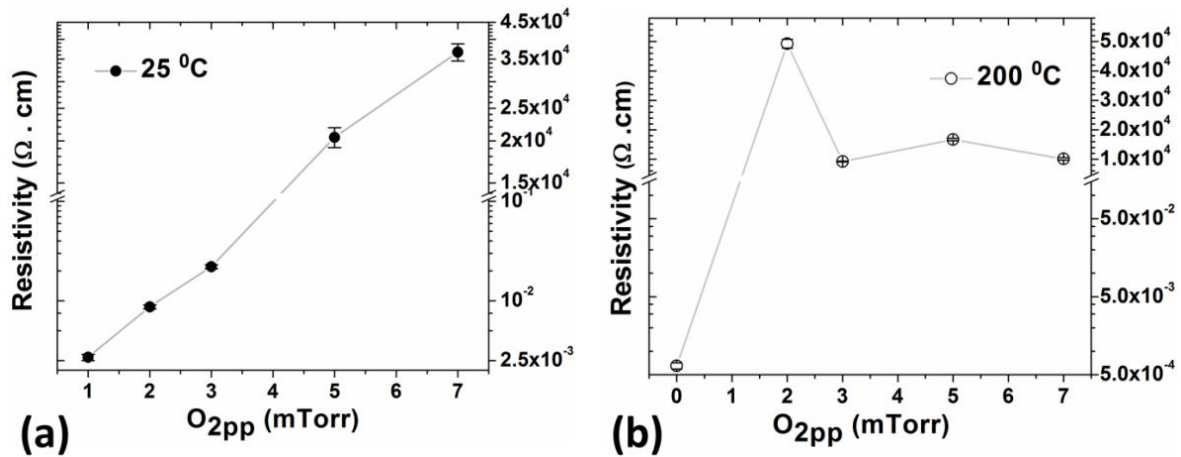


Fig. 6. Variation of Electrical resistivity of as-grown copper oxide thin films onto quartz glass as a function of $\text{O}_{2\text{pp}}$ deposited at $T_{\text{sub}} \approx 25^\circ\text{C}$ (a) and $T_{\text{sub}} \approx 200^\circ\text{C}$ (b).

As can be seen from the Fig. 6a, the resistivities of RT-grown films are found to be monotonically increasing with increasing $\text{O}_{2\text{pp}}$. At $1 \text{ mTorr} \leq \text{O}_{2\text{pp}} \leq 3 \text{ mTorr}$ PLD ambient their resistivities were estimated to be roughly $3 - 24 \text{ m}\Omega \cdot \text{cm}$ which is ~ 3 orders of magnitude lower than the reported resistivity ($40 - 60 \Omega \cdot \text{cm}$) for Cu_2O films grown by PLD above $T_{\text{sub}} \geq 600^\circ\text{C}$ [44]. On the other hand, the resistivities of RT-films with $5 \text{ mTorr} \leq \text{O}_{2\text{pp}} \leq 7 \text{ mTorr}$ PLD ambient are quite high, roughly in the range $20 - 38 \text{ k}\Omega \cdot \text{cm}$ (see Fig. 6a) due to more stoichiometric Cu_2O phase formed in the oxygen rich conditions. In contrast, the resistivity of HT-grown films without injecting O_2 into the PLD chamber was estimated to be

below 7 mΩ.cm (see Fig. 6b). The HT-grown film deposited using $O_{2pp} = 2$ mTorr exhibited the highest resistivity of ~49 kΩ.cm among all samples, due to inclusion of metallic Cu into the Cu₂O matrix which compensates available holes leading to insulating thin films. Since, the PLD chamber provides highly non-equilibrium growth environment to the energetic ablated particles and therefore, the probability to exist metallic Cu as ionized defect states (Cu_i^+) is very high in oxygen poor heated substrate surface. These energetic Cu_i^+ defects compensate available holes leading to insulating thin films compared to the films grown in oxygen rich conditions. Similar observation was reported by X. Liu et al. for PLD grown Cu₂O ($T_{sub} = 600$ °C on MgO(110)) with varying O_{2pp} [26]. In fact, the resistivities of $2 \text{ mTorr} \leq O_{2pp} \leq 7 \text{ mTorr}$ HT-grown films are roughly six orders of magnitude higher than that of the film grown without oxygen. These results are also suggesting that oxygen rich PLD ambient leads to more stoichiometric copper oxide, thereby resulting in more insulating thin films due to the lack of charge carrier creating defect (vacancy type) concentrations.

Hall coefficient measurements and Mott-Schottky plots (see Fig. 7a) constructed from electrochemical impedance spectra [9, 33] were also carried out for samples grown with identical deposition PLD conditions on quartz and ITO substrates respectively (see Fig. S7 in supplementary material). The results together with optical bandgap values are summarized in Table 1. As can be seen, samples grown with $O_{2pp} = 2 - 3$ mTorr, showed a p-type conductivity with appreciable Hall mobility (μ_H) $\sim 4.78 \pm 0.01 \text{ cm}^2 \text{ V}^{-1} \text{ s}^{-1}$ and $\sim 22.20 \pm 0.01 \text{ cm}^2 \text{ V}^{-1} \text{ s}^{-1}$ respectively in RT- and HT-grown PLD Cu₂O films. The higher mobility in HT-grown PLD films could be attributed to the better crystalline and optoelectronic quality evident from XRD, SAED, Raman, and RT-PL analyses. However, the lower carrier concentrations ($\sim 6 \times 10^{12-13} \text{ cm}^{-3}$) of HT-grown films may be attributed to the hole killing [$V_{Cu}^- - V_O^+$] defect complex seen in PL spectra (see Fig. 4b).

Table 1

Optical and Electrical properties of single phase Cu₂O and CuO thin films deposited with low O_{2pp} content during growth.

Growth condition (T _{sub} -O _{2pp})	Band gap (eV)	Thickness (nm) (VASE/ SEM)	Resistivity (Ω.cm)	Carrier density (cm ⁻³) [Hall effect meas.]	Hall Mobility (cm ² /V.s) ± 0.01	Carrier density (cm ⁻³) [EIS meas.]
25_1	1.76	556±21	2.12×10 ⁻³	-3.47×10 ²¹	0.85	-(1.24±.03)×10 ²¹
25_2	1.80	562±4	8.71×10 ⁻³	6.97×10 ²⁰	1.03	-
25_3	2.00	615±25	24.00×10 ⁻³	5.45×10 ¹⁹	4.78	(1.39±.01)×10 ²⁰
200_2	1.90	510±7	49.28×10 ³	5.71×10 ¹²	22.21	-
200_3	2.00	585±7	9.25×10 ³	5.02×10 ¹³	13.45	-
Ann. S1(CuO)	1.50	Assumed ~500	12.2 ± 0.7	-3.42×10 ¹⁷	1.50	-

The acceptor concentration, $N_a \sim 6 \times 10^{12-13} \text{ cm}^{-3}$ and mobility, $\mu_H \sim 13-22 \text{ cm}^2 \text{ V}^{-1} \text{ s}^{-1}$ estimated for T_{sub} ≈ 200 °C(HT) samples are consistent with previous results [6]. The high mobility indicates that PLD films grown at 200 °C possess reasonably good electrical quality, however, a carrier concentration as high as $\sim 10^{14} - 10^{16} \text{ cm}^{-3}$ is desirable for potential Cu₂O based device applications [27]. Therefore, for some specific device applications [3, 26, 45] RT-grown PLD Cu₂O may be utilized.

Notice that carrier density in RT-grown samples is exceptionally high compared to that of HT-grown samples. For example, with O_{2pp} = 2 mTorr, carrier density $\sim (5.71 \pm 0.18) \times 10^{12} \text{ cm}^{-3}$ obtained for HT-grown sample is at least eight orders of magnitude lower than the carrier density $\sim (6.97 \pm 0.01) \times 10^{20} \text{ cm}^{-3}$ for RT-grown samples. With increasing O_{2pp} content slightly to 3 mTorr for RT-grown sample, it was obtained as $\sim (5.45 \pm 0.23) \times 10^{19} \text{ cm}^{-3}$ which is still roughly six orders of magnitude higher than its HT-grown counterpart.

The effective density of states ($D(E_f)$) for these samples are in the range ($D(E_f)$) $\sim 1.35 - 5.67 \times 10^{21} \text{ (eV)}^{-1} \text{ cm}^{-3}$ estimated from EIS data by a similar approach presented in ref. [46] using the equation : $D(E_f) = (C_{sc})^2 / [\epsilon_0 \epsilon_r e^2]$, where, C_{sc} is the space charge capacitance, ϵ_0 is permittivity of free space ($8.854 \times 10^{-12} \text{ F.m}^{-1}$), ϵ_r is the relative dielectric constant (~ 6.6 for Cu_2O [33]) and e is the electronic charge (see supplemental material for detail of the calculations). The high level of N_a , is consistent with low resistivity (few $\text{m}\Omega\text{.cm}$), and low Hall mobilities (μ_H) $\sim 1.03 - 4.78 \text{ cm}^2 \text{V}^{-1} \text{s}^{-1}$ and could be attributed to the scattering of holes at the grain boundaries of these RT-grown nanocrystalline films.

In contrast, the samples grown at 1 mTorr_ 25 °C(RT) exhibited an n-type conductivity with high level of donor concentrations (N_d) $\sim 3.47 \times 10^{21} \text{ cm}^{-3}$ ($\mu_H \sim 0.85 \pm 0.01 \text{ cm}^2 \text{V}^{-1} \text{s}^{-1}$) and $\sim 1.24 \times 10^{21} \text{ cm}^{-3}$ obtained from Hall coefficient measurements and M-S analyses respectively. The effective density of states ($D(E_f)$) for this sample is $1.05 \times 10^{20} \text{ (eV)}^{-1} \text{ cm}^{-3}$ and is slightly lower when compared to p-type RT-grown samples. However, such high level of carrier concentrations may contribute to its exceptionally low resistivity of $\sim 3 \text{ m}\Omega\text{.cm}$. The optical bandgap ($\sim 1.76 \text{ eV}$) of this n-type sample suggests that the donor level may be shallow. In the literature, the Fermi level of donor and acceptor levels for intrinsic Cu_2O is rarely reported ([9],[22] and refs. therein). An approximate band diagram of a PLD-grown Cu_2O thin film electrode is shown in Fig. 7b using electrochemical M-S plot and UV-VIS-NIR optical data to demonstrate the quasi Fermi level energy of E_f^e ($\sim 0.28 \text{ eV}$ below CBM) and E_f^h ($\sim 0.13 \text{ eV}$ above VBM) for donor and acceptor states respectively. The Fermi level is estimated from Flat band potentials -0.72 V vs RHE (Fermi energy with respect to vacuum, $E_f = -3.73 \text{ eV}$) and $+0.91 \text{ V vs RHE}$ ($E_f = -5.37 \text{ eV}$) respectively for n- and p-type $\text{Cu}_2\text{O}/\text{ITO}$ electrodes using a similar approach as described in ref. [9]. The distinct positive- and negative- slope seen in M-S plots in Fig. 7a confirms the n- and p-type conductivity of $\text{Cu}_2\text{O}/\text{ITO}$ electrodes and as seen in Fig. 7b the donor level is obviously located in more positive potentials than the acceptor level for Cu_2O which corroborate the reported results [9, 24] . The estimated $E_f^e \sim 0.28 \text{ eV}$ below the conduction band minimum (CBM) is considerably shallower than the results of Garuthara et al. ($\sim 0.38 \text{ eV}$) [47] and $E_f^h \sim 0.13 \text{ eV}$ above the valence band maximum (VBM) which is slightly small compared to $\sim 0.22 \text{ eV}$ for V_{cu} and $\sim 0.47 \text{ eV}$ for $V_{\text{cu,split}}$ [22] .

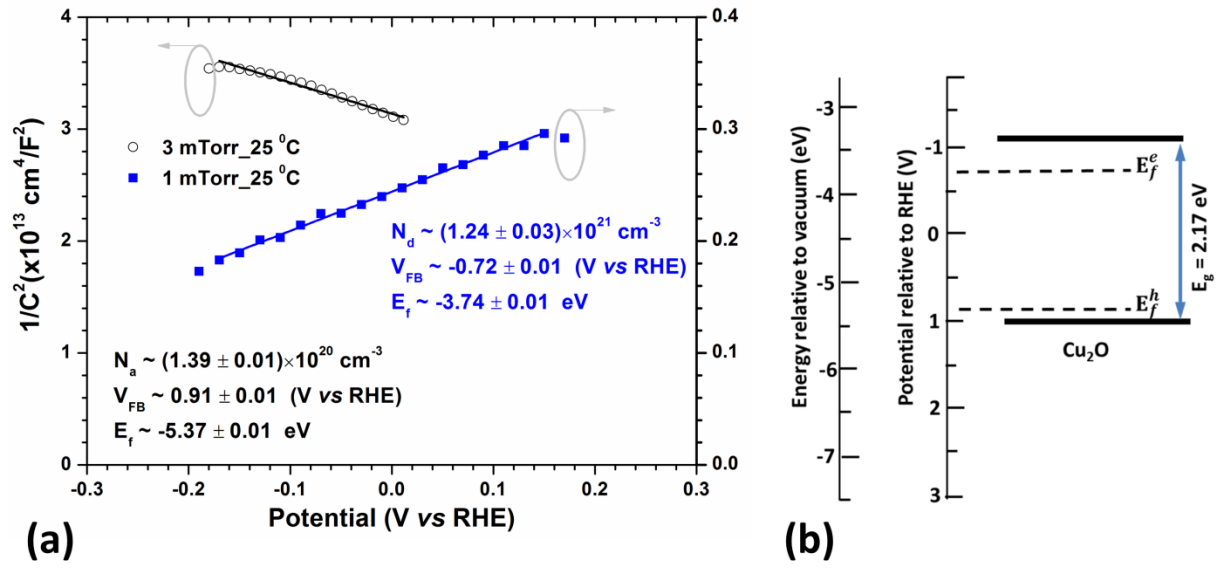


Fig. 7. (a) Mott-Schottky plots of Cu₂O thin films grown on ITO using 1 mTorr_25 °C and 3 mTorr_25 °C deposition conditions showing n-type and p-type conductivity respectively. The estimated carrier concentration, Flat band potential (V_{FB}) and quasi Fermi level energy (E_f^x ; where $x = e$ or h) for donor and acceptor states are also shown in the inset. (b) An approximate band diagram of Cu₂O grown at low O_{2pp} and T_{sub} by PLD.

The low resistivity ($\rho \sim 3 \text{ m}\Omega\cdot\text{cm}$) of n-type Cu₂O thin films grown by PLD is yet at least ~ 3 orders of magnitude above the resistivity of thermally evaporated metallic Cu ($3.5 \text{ }\mu\Omega\cdot\text{cm}$) and Cu+Cu₂O ($27 \text{ }\mu\Omega\cdot\text{cm}$) thin films reported by Figueiredo et al. [30]. Additionally, samples grown at 1 mTorr_25 °C(RT) are single phase Cu₂O, this is evident from both XRD (Fig. 2a) and TEM (Fig. 1a) analyses and they are the most oxygen deficient Cu₂O among the samples deposited in this study. Therefore, the origin of n-type conductivity in these PLD films is presumably due to the electron generating predominant oxygen vacancy (V_o) at the vicinity of Cu/Cu₂O phase boundary [23, 39]. The single phase n-type Cu₂O deposited by electrodeposition with N_d as high as $\sim 10^{20} \text{ cm}^{-3}$ [15] has repeatedly been appeared in the literature, but single phase n-type Cu₂O deposited by PLD is rarely reported. Recently, Xu et al. [11] reported PLD grown phase pure Cu₂O using $O_{2pp} = 0.09 \text{ Pa}$ at $T_{sub} = 600 \text{ }^\circ\text{C}$ with p-type conductivity and they were able to convert them into n-type Cu₂O via post-deposition N₂ plasma treatment. However, in our study the slight increase of O_{2pp} from 1 to 2 mTorr or more in the PLD chamber yielded p-type Cu₂O films suggesting that n-type Cu₂O can only be stabilized in a narrow range of $O_{2pp} \leq 1 \text{ mTorr}$. Our findings for RT-grown samples suggest that critical regulation of low level O_{2pp} helps achieving single phase Cu₂O with tunable optical band gap ($E_g = 1.76 - 2.15 \text{ eV}$) and type of conductivity with appreciable Hall

mobilities ($\mu_H \sim 0.85 - 4.78 \text{ cm}^2 \text{ V}^{-1} \text{ s}^{-1}$). Compared to results reported by Xu et al. this is important for synthesizing diverse optoelectronic device with low thermal budget [3, 45] including p-n Cu_2O based homojunctions [7, 9, 12, 14, 24].

It is conspicuous that estimated acceptor concentrations in RT-grown p-Type Cu_2O samples are also high ($N_a \sim 6 \times 10^{19-20} \text{ cm}^{-3}$) in our observations (see Table 1 and Fig. 7). This is consistent with other recent reports. Theoretical studies reported by Raebiger et al. [16] suggest that the dominant defect V_{Cu} can be above 10^{21} cm^{-3} in concentrations, both in Cu-rich(oxygen poor) and Cu-poor(oxygen rich) growth conditions, to produce a p-type conductivity. Recent experimental works conducted by Zhang et al. [48] reported hole concentrations in the range $5.81 \times 10^{18} - 2.17 \times 10^{21} \text{ cm}^{-3}$ for sputtered Cu_2O thin films grown at room temperatures. Chen et al. [49] also reported that hole concentrations could be as high as $1.5 \times 10^{21} \text{ cm}^{-3}$.

The PLD sample (S1) annealed at 550°C in air for 1 hour is single phase CuO and showed n-type conductivity with carrier concentration $\sim 3.47 \times 10^{17} \text{ cm}^{-3}$ and mobility $\sim 1.5 \text{ cm}^2 \text{ V}^{-1} \text{ s}^{-1}$ and is consistent with reported results [31]. The n-type conductivity of CuO can be understood as follows. PLD grown Cu_2O thin films with high $\text{O}_{2\text{pp}}$ are copper deficient p-type semiconductors where the type of conductivity arises from the copper vacancies can be described by following equation:



where, O_o - oxygen in regular positions of the lattice, V_{Cu}^- - metal vacancies, and h^+ - holes. Due to annealing of p-type Cu_2O in air, more and more oxygen species are escaped from the Cu_2O matrix and generate more Cu^{2+} at the expense of Cu^{1+} in the films (this recrystallizes to a CuO phase) leading to the creation of an electron-generating oxygen vacancy (V_o^{+2}) according to the following equation:



where, V_o^{+2} - oxygen vacancies, and e^- - electrons. As shown in equation (2), evolution of oxygen is accompanied by the formation of oxygen vacancies (with effective positive charge) and electrons that determine n-type of conductivity.

As a proof-of-concept, solid p-n junctions were fabricated with FTO/n-ZnO/p- Cu_2O /Au and p-Si(111)/n- Cu_2O structures. Their stable current-voltage characteristic curves

suggest that p-n junctions were formed successfully, albeit with poor photovoltaic performance. These results are summarized and discussed in the supplementary materials (see Fig. S12 - S14).

4. Conclusions

Single phase n- and p-type Cu₂O thin films were grown on quartz glass and other substrates (ITO, NaCl(100), and p-Si(111)) by a PLD technique and the influence of substrate temperatures and oxygen pressure (O_{2pp}) on the films properties were explored systematically. Thin films grown at 25 °C(RT) and 200 °C(HT) substrate temperatures are single phase Cu₂O with (200) and (111) texture respectively and their texturing is found to be increasing with the increasing oxygen content in the $2 \text{ mTorr} \leq O_{2pp} \leq 5 \text{ mTorr}$ PLD ambient. The optical bandgaps and electrical resistivities of RT-grown Cu₂O thin films were found to be tunable in the range 1.76 eV – 2.15 eV and 3 mΩ.cm – 38 kΩ.cm respectively and both properties were found to be consistently increasing from low to higher values with increasing O_{2pp} due to more stoichiometric Cu(I) phase formation. Critical regulations of low level O_{2pp} during the growth process helps achieving both n- and p-type Cu₂O with appreciable Hall mobilities ($\mu_H \sim 0.85 - 4.78 \text{ cm}^2 \text{ V}^{-1} \text{ s}^{-1}$). The as-grown p- and n-type Cu₂O showed promising rectification in solid junctions with n-ZnO and p-Si electrodes respectively. The findings reported here suggest that critical regulations of PLD growth conditions help achieve single phase Cu₂O growth with tunable electronic properties desirable for diverse optoelectronic applications.

Acknowledgments

S.F.U. Farhad acknowledges the financial help through BANGABANDHU fellowship, Ministry of Science and Technology, Government of Bangladesh to conduct this research. The authors are indebted to Professor Mike Ashfold FRS for allowing his PLD setup located at the Diamond laboratory, School of Chemistry, University of Bristol, UK during the Ph.D. studies. Special thanks are also due to Professor Walther Schawrz, School of Physics, University of Bristol, UK for lending his Kiethley SMU2400 instrument in building a custom-made 4-point collinear probe resistivity measurement setup. S.F.U Farhad also acknowledges the PV characterization support of the Energy Conversion and Storage Research (ECSR) section, Industrial Physics Division, BCSIR Labs, Dhaka, Bangladesh.

Conflict of interest: We declare that we have no conflict of interest.

Author Contributions: S.F.U. Farhad and D.Cherns conceived the idea . D.Cherns supervised the work. S.F.U. Farhad did the experimental works and wrote the manuscript. J.Smith and N. Fox helped with the deposition setup and Hall coefficient measurements. D. Fermín advised on the electrochemical measurements and analyses. All authors contributed to editing and reviewing the final manuscript.

References

- [1] H. Kim, S. Bae, D. Jeon, J. Ryu, Fully solution-processable Cu_2O – BiVO_4 photoelectrochemical cells for bias-free solar water splitting, *Green Chemistry*, 20 (2018) 3732-3742. doi:10.1039/c8gc00681d
- [2] Y.S. Zhi, P.G. Li, P.C. Wang, D.Y. Guo, Y.H. An, Z.P. Wu, X.L. Chu, J.Q. Shen, W.H. Tang, C.R. Li, Reversible transition between bipolar and unipolar resistive switching in $\text{Cu}_2\text{O}/\text{Ga}_2\text{O}_3$ binary oxide stacked layer, *AIP Advances*, 6 (2016) 015215. doi:10.1063/1.4941061
- [3] D. Muñoz-Rojas, M. Jordan, C. Yeoh, A.T. Marin, A. Kursumovic, L.A. Dunlop, D.C. Iza, A. Chen, H. Wang, J.L. MacManus Driscoll, Growth of $\sim 5 \text{ cm}^2\text{V}^{-1}\text{s}^{-1}$ mobility, p-type Copper (I) oxide (Cu_2O) films by fast atmospheric atomic layer deposition (AALD) at 225°C and below, *AIP Advances*, 2 (2012) 042179. doi:10.1063/1.4771681
- [4] H. Zhang, Q. Zhu, Y. Zhang, Y. Wang, L. Zhao, B. Yu, One-Pot Synthesis and Hierarchical Assembly of Hollow Cu_2O Microspheres with Nanocrystals-Composed Porous Multishell and Their Gas-Sensing Properties, *Advanced Functional Materials*, 17 (2007) 2766-2771. doi:10.1002/adfm.200601146
- [5] K. Chen, S. Song, D. Xue, Faceted Cu_2O structures with enhanced Li-ion battery anode performances, *CrystEngComm*, 17 (2015) 2110-2117. doi:10.1039/c4ce02340d
- [6] B.K. Meyer, A. Polity, D. Reppin, M. Becker, P. Hering, P.J. Klar, T. Sander, C. Reindl, J. Benz, M. Eickhoff, C. Heiliger, M. Heinemann, J. Bläsing, A. Krost, S. Shokovets, C. Müller, C. Ronning, Binary copper oxide semiconductors: From materials towards devices, *physica status solidi (b)*, 249 (2012) 1487-1509. doi:10.1002/pssb.201248128
- [7] L.C. Olsen, F.W. Addis, W. Miller, Experimental and theoretical studies of Cu_2O solar cells, *Solar Cells*, 7 (1982) 247-279. doi:10.1016/0379-6787(82)90050-3
- [8] A.E. Rakhshani, Preparation, characteristics and photovoltaic properties of cuprous oxide—a review, *Solid-State Electronics*, 29 (1986) 7-17. doi:10.1016/0038-1101(86)90191-7
- [9] C.M. McShane, K.S. Choi, Junction studies on electrochemically fabricated p-n Cu_2O homojunction solar cells for efficiency enhancement, *Physical chemistry chemical physics : PCCP*, 14 (2012) 6112-6118. doi:10.1039/c2cp40502d
- [10] L. Xiong, S. Huang, X. Yang, M. Qiu, Z. Chen, Y. Yu, p-Type and n-type Cu_2O semiconductor thin films: Controllable preparation by simple solvothermal method and photoelectrochemical properties, *Electrochimica Acta*, 56 (2011) 2735-2739. doi:10.1016/j.electacta.2010.12.054
- [11] M. Xu, X. Liu, W. Xu, H. Xu, X. Hao, X. Feng, Low resistivity phase-pure n-type Cu_2O films realized via post-deposition nitrogen plasma treatment, *Journal of Alloys and Compounds*, 769 (2018) 484-489. doi:10.1016/j.jallcom.2018.08.048

- [12] R.P. Wijesundera, L.K.A.D.D.S. Gunawardhana, W. Siripala, Electrodeposited Cu_2O homojunction solar cells: Fabrication of a cell of high short circuit photocurrent, *Solar Energy Materials and Solar Cells*, 157 (2016) 881-886. doi:10.1016/j.solmat.2016.07.005
- [13] J. Han, J. Chang, R. Wei, X. Ning, J. Li, Z. Li, H. Guo, Y. Yang, Mechanistic investigation on tuning the conductivity type of cuprous oxide (Cu_2O) thin films via deposition potential, *International Journal of Hydrogen Energy*, 43 (2018) 13764-13777. doi:10.1016/j.ijhydene.2018.02.121
- [14] K. Han, M. Tao, Electrochemically deposited p-n homojunction cuprous oxide solar cells, *Solar Energy Materials and Solar Cells*, 93 (2009) 153-157. doi:10.1016/j.solmat.2008.09.023
- [15] P. Wang, H. Wu, Y. Tang, R. Amal, Y.H. Ng, Electrodeposited Cu_2O as Photoelectrodes with Controllable Conductivity Type for Solar Energy Conversion, *The Journal of Physical Chemistry C*, 119 (2015) 26275-26282. doi:10.1021/acs.jpcc.5b07276
- [16] H. Raebiger, S. Lany, A. Zunger, Origins of the p-type nature and cation deficiency in Cu_2O and related materials, *Physical Review B*, 76 (2007). doi:10.1103/PhysRevB.76.045209
- [17] L.Y. Isseroff, E.A. Carter, Electronic Structure of Pure and Doped Cuprous Oxide with Copper Vacancies: Suppression of Trap States, *Chemistry of Materials*, 25 (2013) 253-265. doi:10.1021/cm3040278
- [18] K.P. Musselman, A. Marin, A. Wisnet, C. Scheu, J.L. MacManus-Driscoll, L. Schmidt-Mende, A Novel Buffering Technique for Aqueous Processing of Zinc Oxide Nanostructures and Interfaces, and Corresponding Improvement of Electrodeposited ZnO - Cu_2O Photovoltaics, *Advanced Functional Materials*, 21 (2011) 573-582. doi:10.1002/adfm.201001956
- [19] S.S. Wilson, J.P. Bosco, Y. Tolstova, D.O. Scanlon, G.W. Watson, H.A. Atwater, Interface stoichiometry control to improve device voltage and modify band alignment in $\text{ZnO}/\text{Cu}_2\text{O}$ heterojunction solar cells, *Energy Environ. Sci.*, 7 (2014) 3606-3610. doi:10.1039/c4ee01956c
- [20] M. Pavan, S. Rühle, A. Ginsburg, D.A. Keller, H.-N. Barad, P.M. Sberna, D. Nunes, R. Martins, A.Y. Anderson, A. Zaban, E. Fortunato, $\text{TiO}_2/\text{Cu}_2\text{O}$ all-oxide heterojunction solar cells produced by spray pyrolysis, *Solar Energy Materials and Solar Cells*, 132 (2015) 549-556. doi:10.1016/j.solmat.2014.10.005
- [21] K. Kardarian, D. Nunes, P. Maria Sberna, A. Ginsburg, D.A. Keller, J. Vaz Pinto, J. Deuermeier, A.Y. Anderson, A. Zaban, R. Martins, E. Fortunato, Effect of Mg doping on Cu_2O thin films and their behavior on the $\text{TiO}_2/\text{Cu}_2\text{O}$ heterojunction solar cells, *Solar Energy Materials and Solar Cells*, 147 (2016) 27-36. doi:10.1016/j.solmat.2015.11.041
- [22] D.O. Scanlon, G.W. Watson, Undoped n-Type Cu_2O : Fact or Fiction?, *The Journal of Physical Chemistry Letters*, 1 (2010) 2582-2585. doi:10.1021/jz100962n
- [23] L. Frazer, K.B. Chang, R.D. Schaller, K.R. Poeppelmeier, J.B. Ketterson, Vacancy relaxation in cuprous oxide ($\text{Cu}_{2-x}\text{O}_{1-y}$), *Journal of Luminescence*, 183 (2017) 281-290. doi:10.1016/j.jlumin.2016.11.011
- [24] L.C.-K. Liao, Y.-C. Lin, Y.-J. Peng, Fabrication Pathways of p-n Cu_2O Homo Junction Films by Electrochemical Deposition Processing, *The Journal of Physical Chemistry C*, 117 (2013) 26426-26431. doi:10.1021/jp405715c
- [25] S.F.U. Farhad, R.F. Webster, D. Cherns, Electron microscopy and diffraction studies of pulsed laser deposited cuprous oxide thin films grown at low substrate temperatures, *Materialia*, 3 (2018) 230 - 238. doi:10.1016/j.mtla.2018.08.032
- [26] X. Liu, M. Xu, X. Zhang, W. Wang, X. Feng, A. Song, Pulsed-laser-deposited, single-crystalline Cu_2O films with low resistivity achieved through manipulating the oxygen pressure, *Applied Surface Science*, 435 (2018) 305-311. doi:10.1016/j.apsusc.2017.11.119
- [27] S.H. Wee, P.S. Huang, J.K. Lee, A. Goyal, Heteroepitaxial Cu_2O thin film solar cell on metallic substrates, *Scientific reports*, 5 (2015) 16272. doi:10.1038/srep16272

- [28] S. Ishizuka, K. Akimoto, Control of the growth orientation and electrical properties of polycrystalline Cu_2O thin films by group-IV elements doping, *Applied Physics Letters*, 85 (2004) 4920. doi:10.1063/1.1827352
- [29] S. Nandy, R. Thapa, M. Kumar, T. Som, N. Bundaleski, O.M.N.D. Teodoro, R. Martins, E. Fortunato, Efficient Field Emission from Vertically Aligned $\text{Cu}_2\text{O}_{1-\delta}(111)$ Nanostructure Influenced by Oxygen Vacancy, *Advanced Functional Materials*, 25 (2015) 947-956. doi:10.1002/adfm.201402910
- [30] V. Figueiredo, E. Elangovan, G. Gonçalves, P. Barquinha, L. Pereira, N. Franco, E. Alves, R. Martins, E. Fortunato, Effect of post-annealing on the properties of copper oxide thin films obtained from the oxidation of evaporated metallic copper, *Applied Surface Science*, 254 (2008) 3949-3954. doi:10.1016/j.apsusc.2007.12.019
- [31] X. Hu, F. Gao, Y. Xiang, H. Wu, X. Zheng, J. Jiang, J. Li, H. Yang, S. Liu, Influence of oxygen pressure on the structural and electrical properties of CuO thin films prepared by pulsed laser deposition, *Materials Letters*, 176 (2016) 282-284. doi:10.1016/j.matlet.2016.04.055
- [32] N. Gupta, R. Singh, F. Wu, J. Narayan, C. McMillen, G.F. Alapatt, K.F. Poole, S.-J. Hwu, D. Sulejmanovic, M. Young, G. Teeter, H.S. Ullal, Deposition and characterization of nanostructured Cu_2O thin-film for potential photovoltaic applications, *Journal of Materials Research*, 28 (2013) 1740-1746. doi:10.1557/jmr.2013.150
- [33] A. Paracchino, J.C. Brauer, J.-E. Moser, E. Thimsen, M. Graetzel, Synthesis and Characterization of High-Photoactivity Electrodeposited Cu_2O Solar Absorber by Photoelectrochemistry and Ultrafast Spectroscopy, *The Journal of Physical Chemistry C*, 116 (2012) 7341-7350. doi:10.1021/jp301176y
- [34] S.F.U. Farhad, M.M. Hossain, N.I. Tanvir, S. Islam, Texture and Bandgap Tuning of Phase Pure Cu_2O Thin Films Grown By a Simple Potentiostatic Electrodeposition Technique, *ECS Meeting Abstracts*, MA2020-01 (2020) 1212-1212. doi:10.1149/ma2020-01191212mtgabs
- [35] S.F.U. Farhad, M.A. Hossain, N.I. Tanvir, R. Akter, M.A.M. Patwary, M. Shahjahan, M.A. Rahman, Structural, optical, electrical, and photoelectrochemical properties of cuprous oxide thin films grown by modified SILAR method, *Materials Science in Semiconductor Processing*, 95 (2019) 68-75. doi:10.1016/j.mssp.2019.02.014
- [36] M.Y. Ghotbi, Z. Rahmati, Nanostructured copper and copper oxide thin films fabricated by hydrothermal treatment of copper hydroxide nitrate, *Materials & Design*, 85 (2015) 719-723. doi:10.1016/j.matdes.2015.07.081
- [37] S.F.U. Farhad, Copper Oxide Thin Films grown by Pulsed Laser Deposition for Photovoltaic Applications, in: *School of Physics, University of Bristol, UK, January 2016*, pp. 222. <https://ethos.bl.uk/OrderDetails.do?uin=uk.bl.ethos.691178>
- [38] K. Wang, W. Gao, H.W. Zheng, F.Z. Li, M.S. Zhu, G. Yang, G.T. Yue, Y.K. Liu, R.K. Zheng, Heteroepitaxial growth of Cu_2O films on Nb-SrTiO_3 substrates and their photovoltaic properties, *Ceramics International*, 43 (2017) 16232-16237. doi:10.1016/j.ceramint.2017.08.205
- [39] O. Porat, I. Riess, Defect chemistry of Cu_{2-y}O at elevated temperatures. Part II: Electrical conductivity, thermoelectric power and charged point defects, *Solid State Ionics*, 81 (1995). doi:10.1016/0167-2738(95)00169-7
- [40] Y. Wang, P. Miska, D. Pilloud, D. Horwat, F. Mücklich, J.F. Pierson, Transmittance enhancement and optical band gap widening of Cu_2O thin films after air annealing, *Journal of Applied Physics*, 115 (2014) 073505. doi:10.1063/1.4865957
- [41] Syed Farid Uddin Farhad, David Cherns, Structural, Optical and Electrical properties of nanocrystalline Cu_2O thin films grown by Pulsed Laser Deposition, Paper# 9AM-J8.30 Abstract book document# 1868681 in: *2014 MRS Spring Meeting and Exhibition, Material Research Society(MRS), San Francisco, California, USA*. <http://dx.doi.org/10.17632/whksg7scsx.1>

- [42] L. Debbichi, M.C. Marco de Lucas, J.F. Pierson, P. Krüger, Vibrational Properties of CuO and Cu₄O₃ from First-Principles Calculations, and Raman and Infrared Spectroscopy, *The Journal of Physical Chemistry C*, 116 (2012) 10232-10237. doi:10.1021/jp303096m
- [43] S.F.U. Farhad, N.I. Tanvir, M.S. Bashar, M.S. Hossain, M. Sultana, N. Khatun, Facile synthesis of oriented zinc oxide seed layer for the hydrothermal growth of zinc oxide nanorods, *Bangladesh Journal of Scientific and Industrial Research*, 53 (2018) 233. doi:10.3329/bjsir.v53i4.39186
- [44] S.B. Ogale, P.G. Bilurkar, N. Mate, S.M. Kanetkar, N. Parikh, B. Patnaik, Deposition of copper oxide thin films on different substrates by pulsed excimer laser ablation, *Journal of Applied Physics*, 72 (1992) 3765-3769. doi:10.1063/1.352271
- [45] A. Subramanian, J.D. Perkins, R.P. O'Hayre, S. Lany, V. Stevanovic, D.S. Ginley, A. Zakutayev, Non-equilibrium deposition of phase pure Cu₂O thin films at reduced growth temperature, *APL Materials*, 2 (2014) 022105. doi:10.1063/1.4865457
- [46] B. Bera, A. Chakraborty, T. Kar, P. Leuaa, M. Neergat, Density of States, Carrier Concentration, and Flat Band Potential Derived from Electrochemical Impedance Measurements of N-Doped Carbon and Their Influence on Electrocatalysis of Oxygen Reduction Reaction, *The Journal of Physical Chemistry C*, 121 (2017) 20850-20856. doi:10.1021/acs.jpcc.7b06735
- [47] R. Garuthara, W. Siripala, Photoluminescence characterization of polycrystalline n-type Cu₂O films, *Journal of Luminescence*, 121 (2006) 173-178. doi:10.1016/j.jlumin.2005.11.010
- [48] L. Zhang, L. McMillon, J. McNatt, Gas-dependent bandgap and electrical conductivity of Cu₂O thin films, *Solar Energy Materials and Solar Cells*, 108 (2013) 230-234. doi:10.1016/j.solmat.2012.05.010
- [49] X. Chen, D. Parker, M.-H. Du, D.J. Singh, Potential thermoelectric performance of hole-doped Cu₂O, *New Journal of Physics*, 15 (2013) 043029. doi:10.1088/1367-2630/15/4/043029

Supplementary Material

Pulsed laser deposition of single phase n- and p-type Cu_2O thin films with low resistivity

Syed Farid Uddin Farhad^{1,2,3,4*}, David Cherns¹, James Smith², Neil Fox^{1,2}, and David Fermín³

¹H.H. Wills Physics Laboratory, School of Physics, University of Bristol, BS8 1TL, UK

²Diamond Laboratory, School of Chemistry, University of Bristol, BS8 1TS, UK

³Electrochemistry Laboratory, School of Chemistry, University of Bristol, BS8 1TS, UK

⁴Industrial Physics Division, BCSIR Labs, Dhaka, Bangladesh Council of Scientific and Industrial Research (BCSIR), Dhaka 1205, Bangladesh

*Corresponding Author: sf1878@my.bristol.ac.uk ; s.f.u.farhad@bcsir.gov.bd

Copper oxide films grown with $\text{O}_{2\text{pp}} = 10$ and 3 mTorr at $T_{\text{sub}} = 25 - 400^\circ\text{C}$:

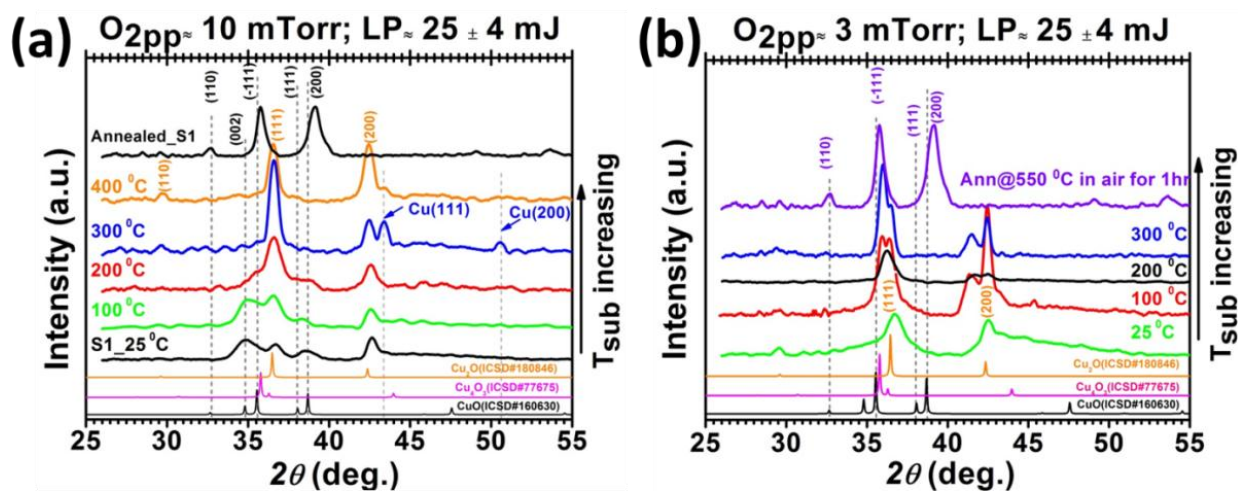


Fig. S1. (color online) XRD patterns (vertically offset for clarity) of copper oxide thin films deposited onto quartz substrate with a constant laser pulse energy ($LP \approx 25 \pm 4$ mJ) using (a) $\text{O}_{2\text{pp}} = 10$ mTorr, and (b) $\text{O}_{2\text{pp}} = 3$ mTorr as a function of substrate temperature. The dotted and solid vertical lines indicate the Bragg reflection peaks of CuO and Cu respectively.

$O_{2pp} = 10$ mTorr:

Thin films deposited at $T_{sub} \approx 100$ °C, show a mixture of CuO and Cu₂O phases. In contrast, films grown at $T_{sub} \geq 200$ °C exhibit strong Cu₂O(111) and Cu₂O(200) reflection peaks but no clear evidence of CuO and Cu₄O₃ phases (see the respective ICSD patterns given in the figure). For films grown at $T_{sub} \geq 300$ °C, there is also evidence of metallic Cu with (111) and (200) planes in XRD patterns. In addition, Cu₂O phase is seen to be increasing with the expense of CuO phase, suggesting that an elevated temperature might be more favourable for PLD ablated adatoms to form single phase Cu₂O but it also suggests that even $O_{2pp} = 10$ mTorr is not enough to suppress Cu within 300 °C $\leq T_{sub} \leq 400$ °C regime (see blue and orange curve in Fig. S1a). The likely reason of the absence of CuO but the presence of Cu₂O and Cu most probably due to the dissolving of O species from the Cu-O films in 300 °C $\leq T_{sub} \leq 400$ °C regime. These results suggest that scope of controlling the phase purity is less certain in case the of oxygen rich PLD ambient.

$O_{2pp} = 3$ mTorr:

Thin films deposited at $T_{sub} \approx 25$ °C, exhibit strong Cu₂O only with (111) and (200) but those grown at 100 °C $\leq T_{sub} \leq 300$ °C contains Cu₂O phase along with Cu_xO_y [1].

Cu₂O films grown at $T_{sub} = 25$ °C on amorphous, polycrystalline and crystalline substrate:

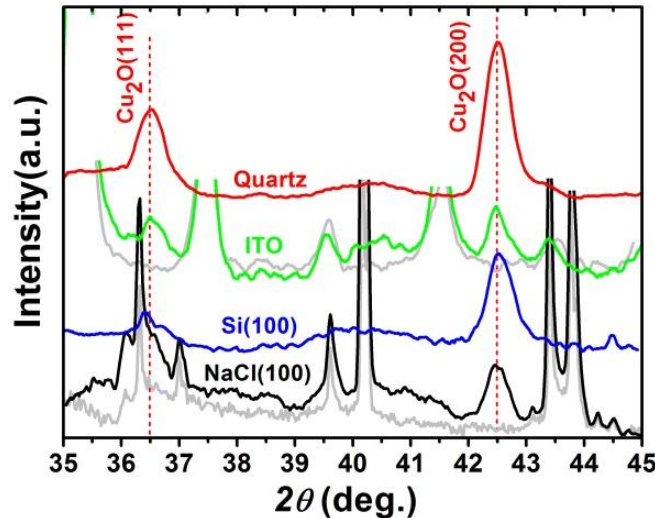


Fig. S1.1. (color online) XRD patterns (vertically offset for clarity) of Cu₂O films deposited on various substrates at $O_{2pp} = 5$ mTorr, $T_{sub} \approx 25$ °C. XRD from blank ITO and NaCl(100) substrates are shown by faded curves and included in the graph for comparison purposes. Reference peak positions of pure Cu₂O are indicated by vertical dotted lines.

Clearly, XRD patterns of thin films deposited on quartz glass, polycrystalline ITO, (100) oriented Si and (100) oriented NaCl substrate revealed that all films are polycrystalline in nature irrespective of the type of substrate used. These diffractogram exhibit 111 and 200 reflections of Cu_2O phase with an average lattice parameter, $a \sim 4.26 \pm 0.02 \text{ \AA}$ (cf. $a \sim 4.27 \text{ \AA}$ for bulk Cu_2O), no evidence of other Cu, Cu_4O_3 and CuO phases. Phase pure Cu_2O films grown at $T_{\text{sub}} \approx 25^\circ\text{C}$ on (100) oriented substrates exhibit 200 texturing as evident from Fig. S1.1.

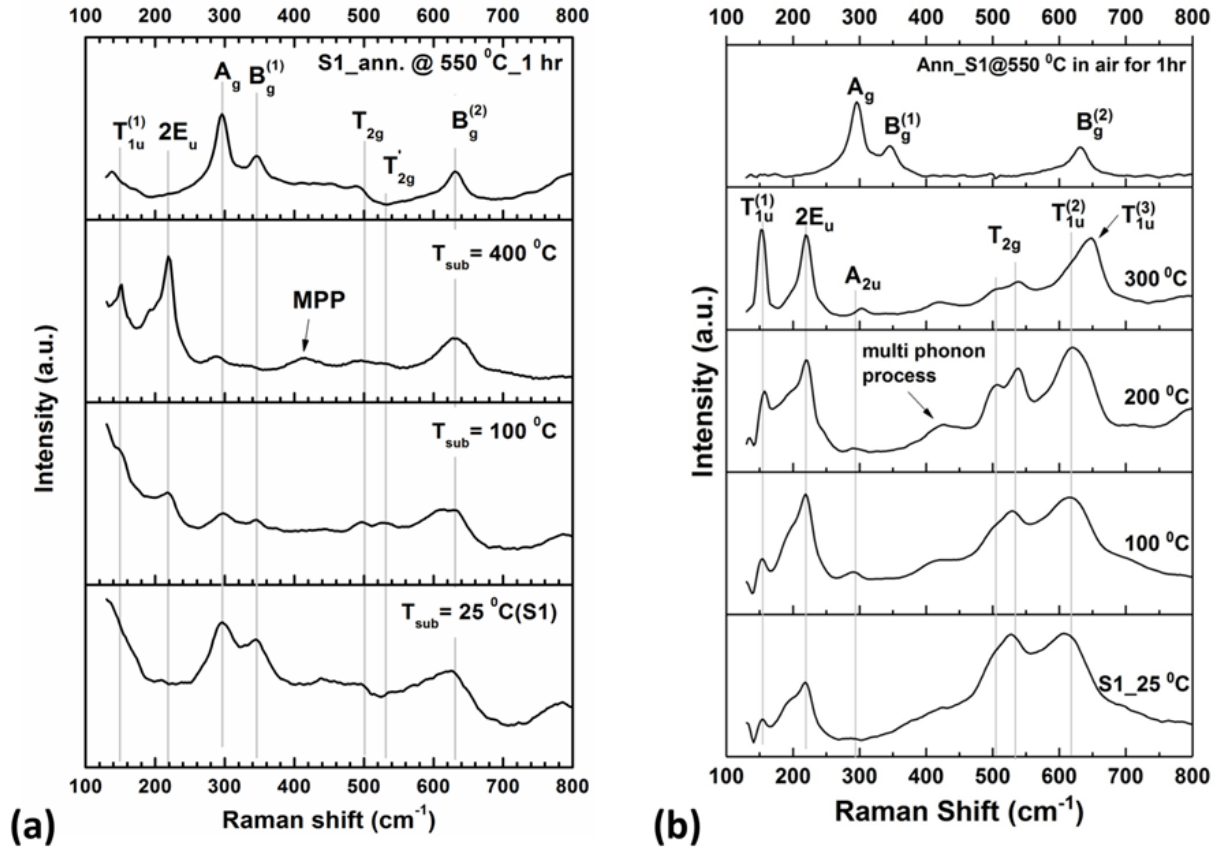


Fig. S2. Raman spectra of copper oxide thin films deposited onto quartz substrate with a constant laser pulse energy ($LP \approx 25 \pm 4 \text{ mJ}$) using (a) $\text{O}_{2\text{pp}} = 10\text{mTorr}$, and $\text{O}_{2\text{pp}} = 3\text{mTorr}$ (b) as a function of substrate temperature. The vertical lines indicate the reference vibrational modes of copper oxide [1,2].

In order to understand the crystallographic nature of PLD grown Cu_2O films, texture coefficient (Fig. S3a), and crystallite size (Fig. S3b) were analysed as a function of $\text{O}_{2\text{pp}}$ in both RT- and HT-grown films. Texturing coefficient (f) is calculated from the following formula [2] considering (111) and (200) are the only planes lying parallel to the substrate and hence diffracting strongly:

$$f = 1 - 2y/(x + y) \quad (\text{S1})$$

where, $x = \frac{I(111)}{I(200)}$, $y = \frac{I_0(111)}{I_0(200)}$; $I(\text{hkl})$ and $I_0(\text{hkl})$ are the intensities of (hkl) X-ray reflection planes of as grown thin films and bulk Cu_2O respectively. (XRD of bulk Cu_2O powder scrapped off from PLD target is shown in Fig. S7.1 below). When $f \rightarrow -1$, thin films are highly (200) textured and crystallites are dominantly (111) orientated when $f \rightarrow 1$. One can see that the RT- and HT-grown films approached towards highly {100} and {111} texturing, respectively, with increasing $\text{O}_{2\text{pp}}$ up to 7 mTorr.

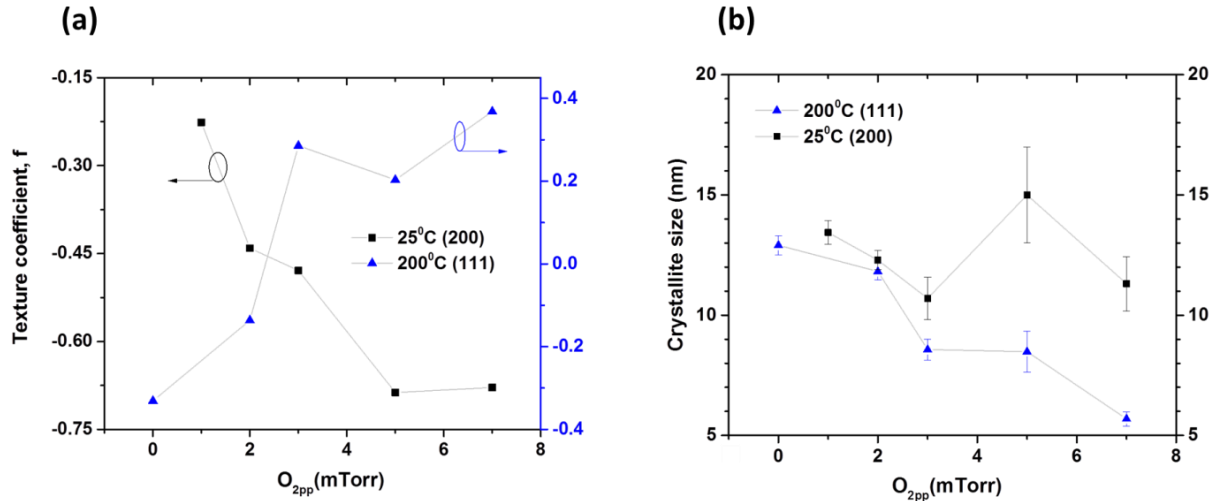


Fig. S3. Texture coefficient (a), and average crystallite domain size(b) of Cu_2O films deposited at $T_{\text{sub}} \approx 25^\circ\text{C}$ (denoted by ■) and $T_{\text{sub}} \approx 200^\circ\text{C}$ (denoted by ▲) as a function of $\text{O}_{2\text{pp}}$.

Fig. S3b shows the variation of the average crystallites domain size as a function of $\text{O}_{2\text{pp}}$. Both for RT- and HT-grown films, grain growth is negatively affected with increasing $\text{O}_{2\text{pp}}$; for example, in case of HT-grown films, crystallite size start to decrease monotonically from ~12 nm with no $\text{O}_{2\text{pp}}$ down to ~5 nm with $\text{O}_{2\text{pp}} \approx 7$ mTorr; suggesting that $\text{O}_{2\text{pp}}$ must have greater impact on controlling growth rate as well as films microstructure. The likely reason is that higher level

of O_{2pp} present during PLD scatter, attenuate and thermalize the ablation plume; consequently lowering the kinetic energy of particle arriving the substrate surface. Therefore, the lower the kinetic energy of adatoms, the slower the grain growth as well as the deposition rate. Furthermore, the crystallite size in HT-grown films are always found to be smaller than those of the RT-grown films irrespective of the O_{2pp} level, indicating that the growth rate in RT-films is faster than HT-films, which corroborates the results presented Fig. 6 of the main text.

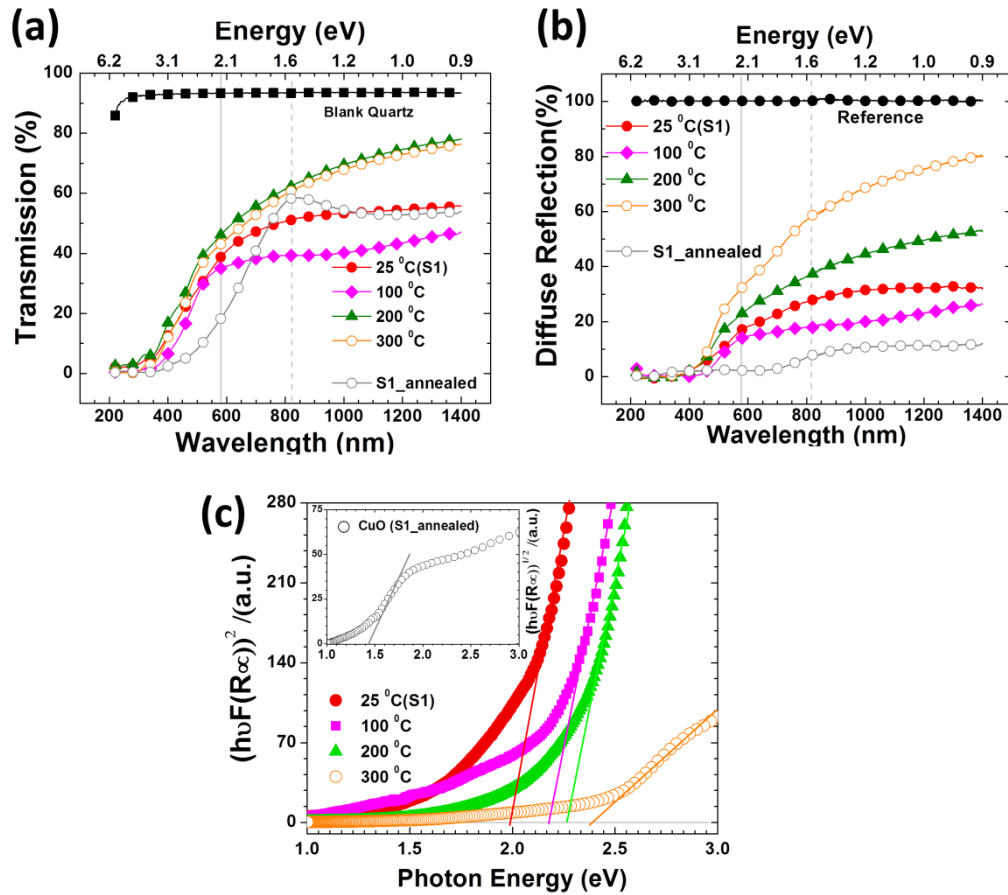


Fig. S4. (color online) Transmission (a), diffuse reflection (b) and Tauc plot (c) of PLD grown Cu_2O films as a function of substrate temperature. Tauc plot of the CuO (S1_annealed) film is shown in the inset.

PLD films grown at $O_{2pp} = 3$ mTorr, $T_{sub} = 300$ °C contain predominant Cu_xO_y phase (see Fig. S1b) and exhibited a larger bandgap (E_g) ~ 2.45 eV (direct) compared to single phase Cu_2O film ($E_g = 1.96$ - 2.20 eV) and RT-grown sample (S1) annealed in air at 550 °C for 1 hour exhibited a bandgap ~ 1.45 eV (indirect) due to complete conversion to CuO.

The electrical resistivity measured by four point collinear probe exhibited gradual increase in resistivity with increasing substrate temperature at a fixed O_{2pp} . Fig. S5 (below) shows the variation of resistivity (denoted by solid circle (●)) and thickness (denoted by solid rectangle (■)) as a function of T_{sub} at constant $O_{2pp} = 3$ mTorr. At fixed $O_{2pp} = 3$ mTorr, the RT(25 °C) -grown film exhibited ~ 6 orders of magnitude lower resistivity (23 ± 1 m Ω .cm) than those of the films grown at 100 °C $\leq T_{sub} \leq 300$ °C (their resistivities are found in the range 5 – 30 k Ω .cm).

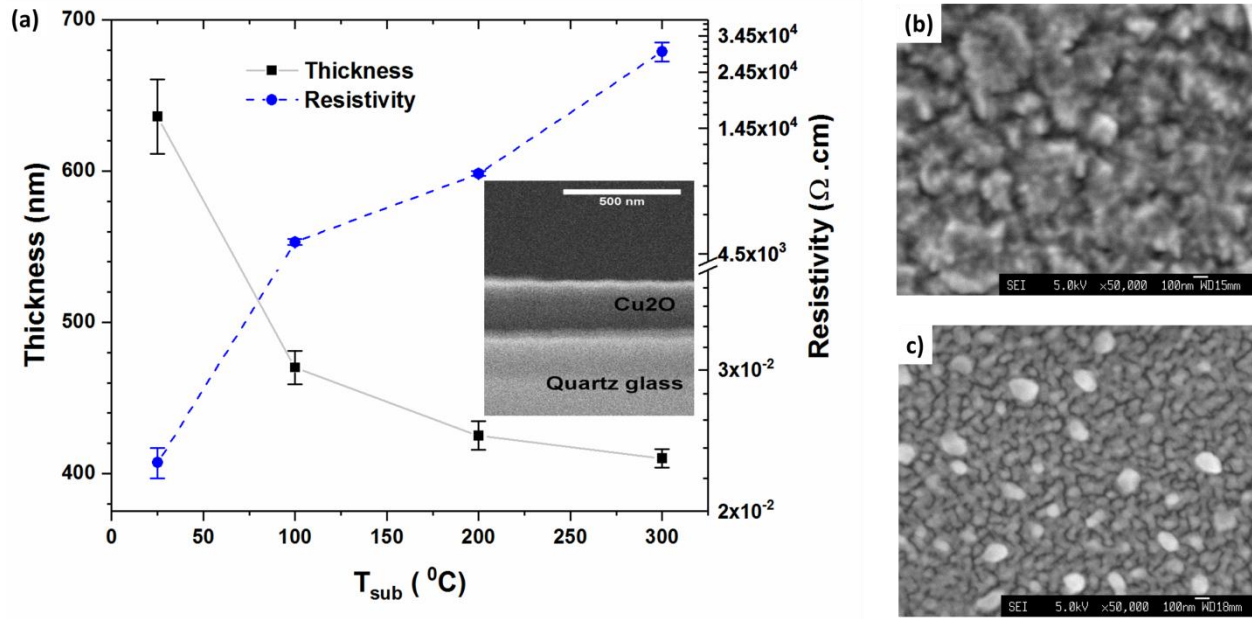


Fig. S5. Variation in electrical resistivity and thickness of Cu_2O thin film grown at $O_{2pp} = 3$ mTorr as a function of substrate temperature (a); Plane SEM view of Cu_2O film deposited at $T_{sub} \approx 25$ °C (b) and at $T_{sub} \approx 300$ °C (c). The thickness data presented in (a) are the average value of VASE and SEM measurements (inset shows a typical cross-sectional SEM view of a sample grown at $T_{sub} \approx 300$ °C).

Notice the film thickness is consistently decreasing from $\sim 635 \pm 25$ nm to $\sim 410 \pm 6$ nm when substrate temperature is elevated from $T_{sub} = 25$ °C(RT) to $T_{sub} = 300$ °C. The estimated film thickness of Cu_2O with 2 mTorr $\leq O_{2pp} \leq 7$ mTorr was found to be roughly in the range 550 – 625 nm and 500 – 600 nm for 25 °C - and 200 °C -grown films respectively (data not shown here)). Intriguingly, grains in RT-grown film are significantly larger than those of $T_{sub} \approx 300$ °C-grown films as evident from SEM micrographs (cf. Fig. S5b and S5c), suggesting that the columnar like grain (with a large density of voids) growth in the former and lateral growth in the latter might be playing a vital role in decreasing growth rate with increasing growth temperature. The higher resistivity of thin films grown at elevated T_{sub} suggesting that samples being investigated are in general more oxygen rich as well as stoichiometric compared to RT(25 °C)-

grown thin films. This observation corroborates the analyses results of XRD and PL (see Fig. 2 and Fig. 4 in the main text).

Surface morphology of PLD grown Copper oxide thin films on different substrates:

The FE-SEM investigated surface morphologies of copper-oxide thin films grown on quartz glass, ITO, NaCl(100), and AZO substrates at various deposition and processing conditions are presented below:

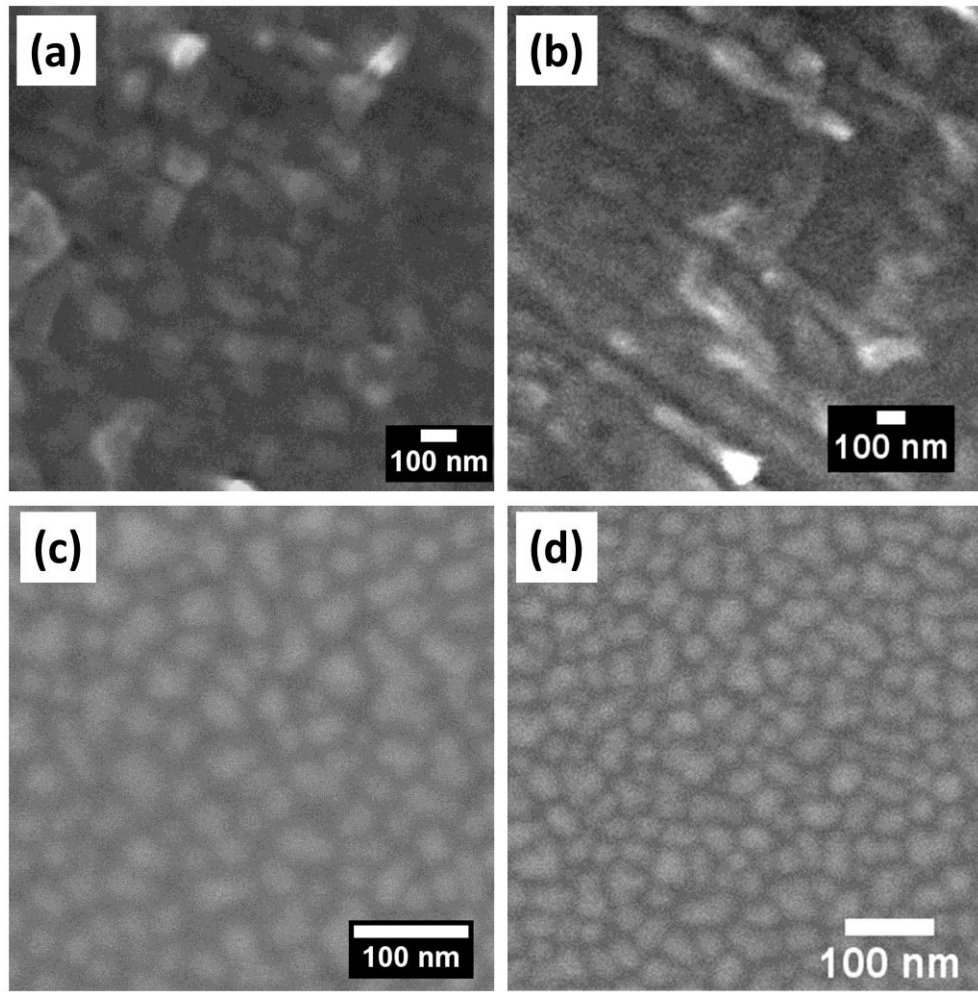


Fig. S5.1. SEM micrographs of copper oxide thin films deposited at (a) $O_{2pp} = 1$ mTorr_ $T_{sub} \approx 25$ °C , (b) $O_{2pp} = 3$ mTorr_ $T_{sub} \approx 25$ °C and (c) $O_{2pp} \ll 1$ mTorr_ $T_{sub} \approx 200$ °C and (d) $O_{2pp} \ll 1$ mTorr_ $T_{sub} \approx 300$ °C on quartz glass.

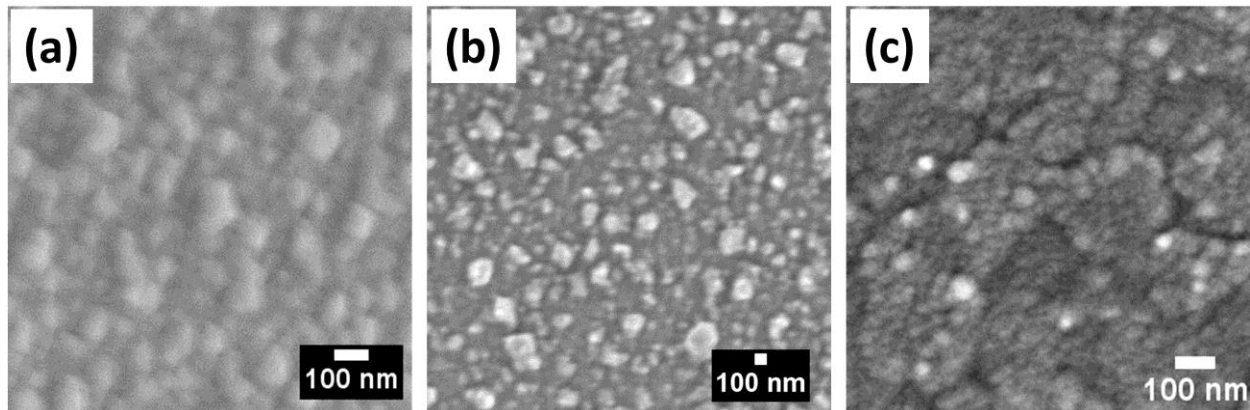


Fig. S5.2. SEM micrographs of Cu_2O thin films deposited at $T_{\text{sub}} \approx 25^\circ\text{C}$ with (a) 2 mTorr $\text{O}_{2\text{pp}}$ and (b) 5 mTorr $\text{O}_{2\text{pp}}$ onto commercial ITO coated soda lime glass (c).

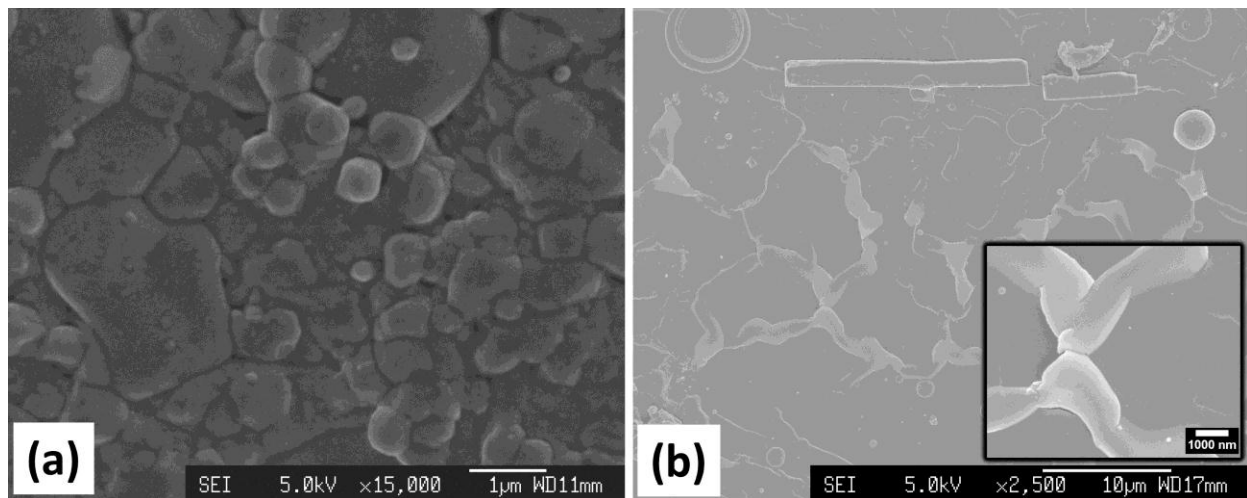


Fig. S5.3: SEM micrographs of Cu_2O thin films (a) deposited with $\text{O}_{2\text{pp}} = 5$ mTorr, $\text{LP} \approx 30 \pm 2$ mJ at $T_{\text{sub}} \approx 200^\circ\text{C}$ on $\text{NaCl}(100)$ substrate (b). A magnified image of the blank $\text{NaCl}(100)$ are shown in the right figure with scale bar $1\ \mu\text{m}$.

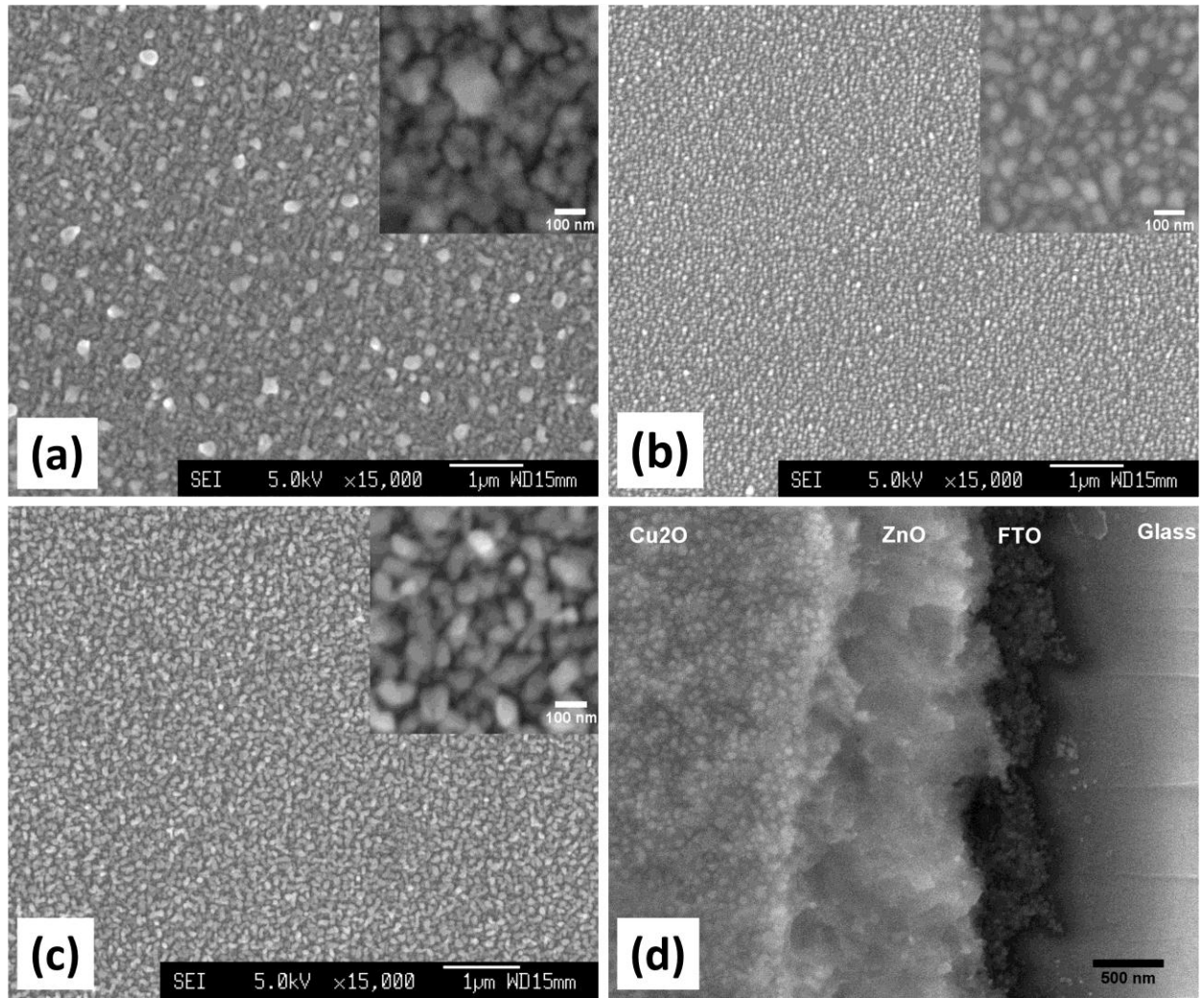


Fig. S5.4. SEM (Plane view) micrographs of Cu_xO_y thin films grown at $T_{\text{sub}} \approx 300^\circ\text{C}$ with (a) 3 mTorr $\text{O}_{2\text{pp}}$, (b) 5 mTorr $\text{O}_{2\text{pp}}$, and (c) 10 mTorr $\text{O}_{2\text{pp}}$, respectively onto Al-doped ZnO coated (PLD grown at 10 mTorr_ $T_{\text{sub}} \approx 400^\circ\text{C}$) soda lime glass. Deposition time ~ 45 min for samples (a) – (c). (d) SEM (cross-sectional view, $\sim 7^\circ$ tilted) micrograph of Cu_xO_y thin films grown at 3 mTorr $\text{O}_{2\text{pp}}$ _ $T_{\text{sub}} \approx 300^\circ\text{C}$ (Deposition time ~ 45 min) onto ZnO coated (PLD grown at 10 mTorr_ $T_{\text{sub}} \approx 300^\circ\text{C}$, Deposition time 30 min) FTO glass.

XRD of Cu_2O ceramic PLD target (purity $\sim 99.95\%$) and ICSD powder diffraction files of Cu_2O , Cu_4O_3 and CuO phases:

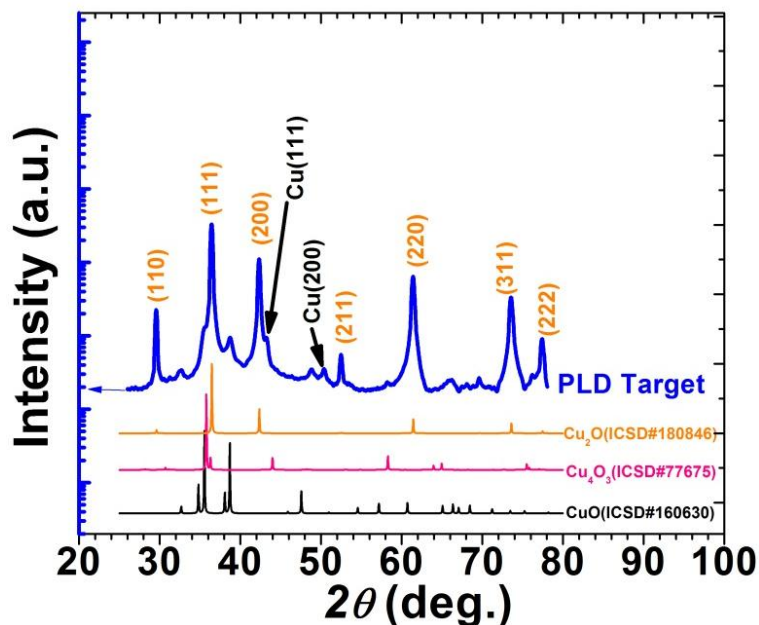


Fig. S7.1. (color online) XRD patterns of PLD target used for deposition of copper oxide thin films (log scaled indicating by arrow in the left) together with standard ICSD patterns of three different copper-oxide compounds (linear vertical scale in the right).

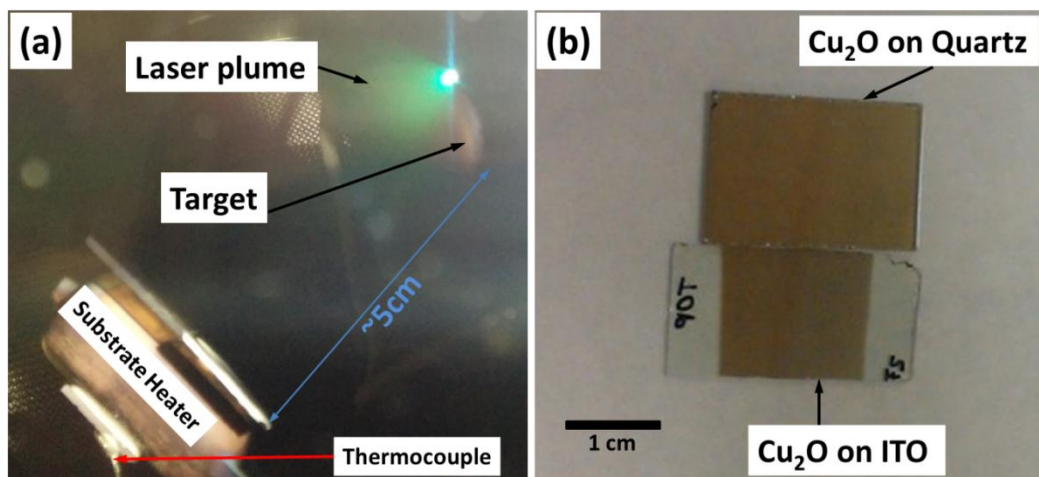


Fig. S7. (a) Photograph taken during the synthesis of Cu_2O film on two different substrates in a single deposition session. (b) Photograph of Cu_2O thin films on ITO and Quartz substrate after deposition. Part of ITO was masked with PTFE tape during deposition for selective ohmic contact required for subsequent electrochemical impedance measurements.

Hall mobility measurements:

Measurements of the Hall voltage and sheet resistance of samples were carried out using the van der Pauw configuration as per the standard procedure set out by NIST Physical Measurement Laboratory [3]. Hall voltage measurements were performed using a 1 Tesla (T) permanent magnet, with the polarity of the magnetic field (B(+) and B(-)) being reversed manually through sample stage orientation relative to the magnetic field. All measurements were taken by sourcing a range of currents and measuring the voltage change (see inset in Fig. S8 (left)). The resultant voltage step functions allow the offset voltage to be measured and taken into account when calculating the Hall voltage and mobilities. The offset voltage is typically a product of non-ideal Ohmic contact, asymmetric contact placement, or irregular sample shape. Joule heating of the sample during testing was also reduced by using the minimum permitted source current thereby minimising the thermal contribution in the measurement, following the ASTM recommendation ref: F46. All electrical measurements were performed at room temperature within a light-tight Faraday cage.

Hall voltages, V_H , were measured with varying source current, I . The four measurement configurations were averaged to form (V_H/I) which was used for calculating mobility via the equation, $\mu_H = (V_H/I) \times 10^4 \times B^{-1} \times (R_s)^{-1}$, where magnetic field B is in T and R_s is the sheet resistance in ohm/square. The large offset voltage (Fig. S10) seen in the measurements were subtracted to reveal the actual V_H . R_s values measured in 4-point probe were found to be of the order of $\pm 2-5\%$ of that of the van der Pauw measurements, this is thought to be primarily due to the different nature of the electrical contact arrangement and the sample size.

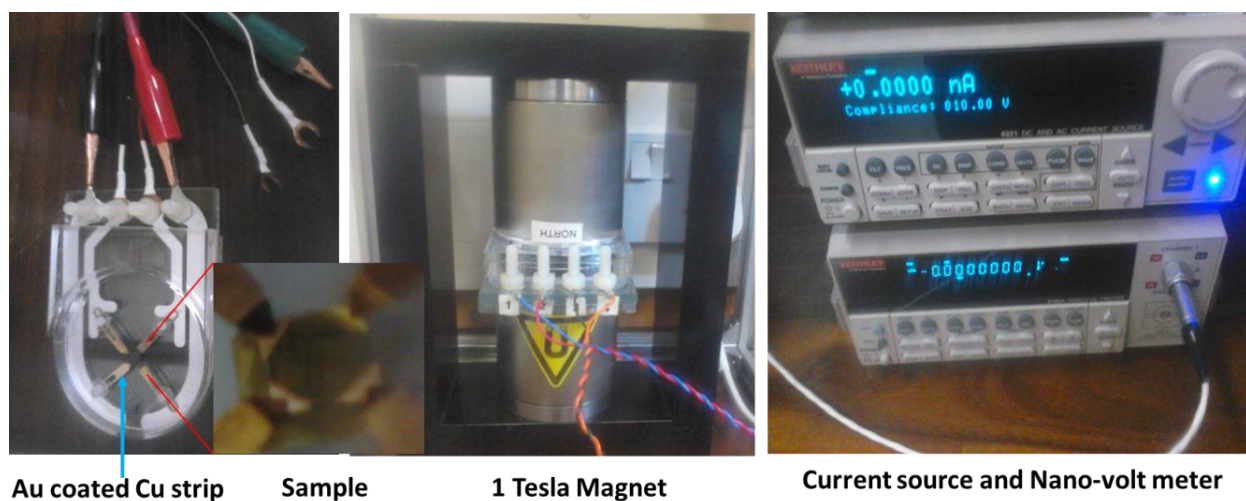


Fig. S8. (color online) A precision home-built Hall mobility measurement setup used in this study.

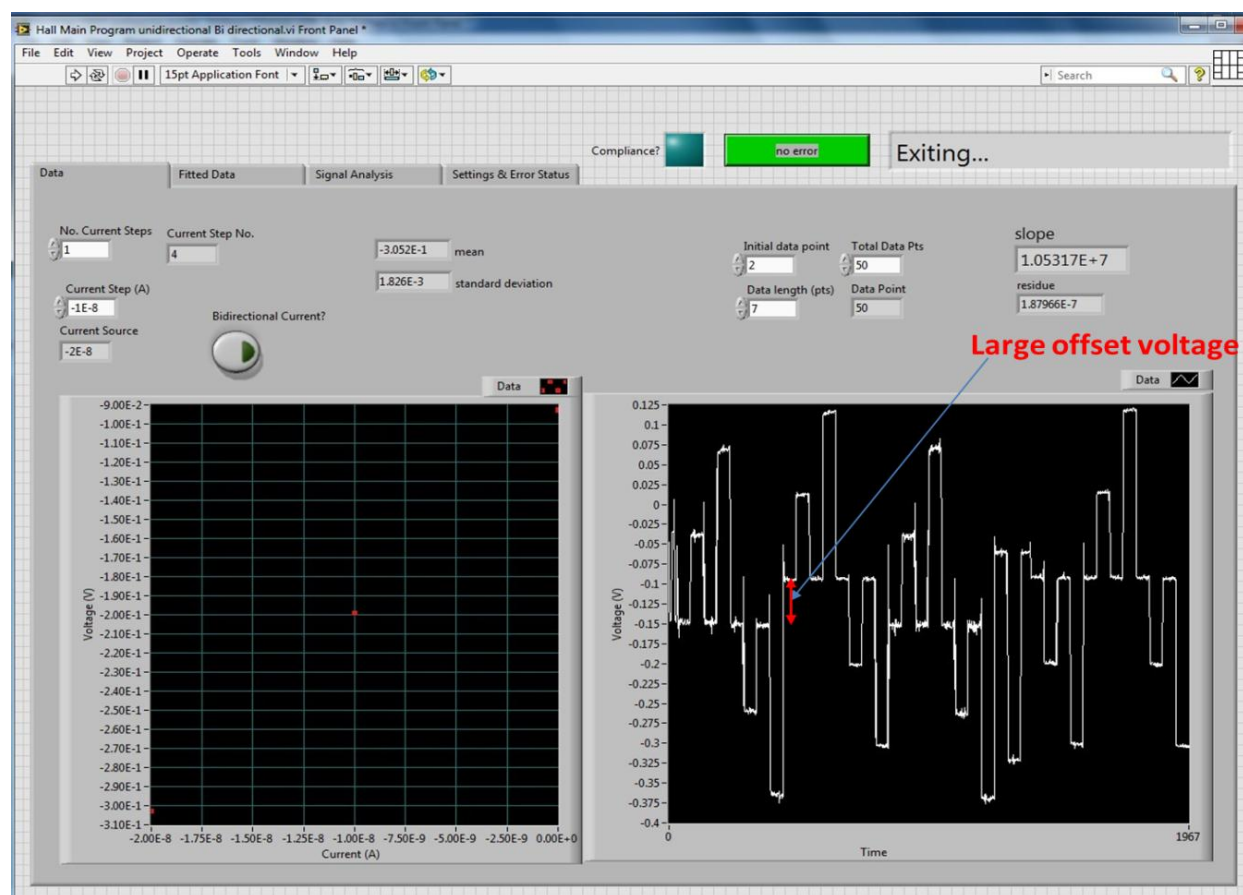


Fig. S9. (color online) An example of a large offset voltage (LabVIEW program display) in a typical Hall measurement setup due to non-ideal contact and sample shape.

Electrochemical Impedance Spectroscopy (EIS):

To evaluate electrochemical impedance parameter the frequency response analysis (FRA) was performed by applying a set of constant bias voltage over a narrow potential window (-0.25 to 0.05 V vs RHE) as mentioned in the experimental section 2, and a standby potential ca. 0.01 V (vs RHE) was maintained after each measurement to avoid possible formation of native CuO atop the film. This was confirmed by doing CV before and after FRA as shown Fig. S10 evident from the low capacitive current (few μA) within the potential scanning range. It is worth mentioning here that the experimental electrochemical impedance parameters are fitted to a suitable RQ (Q is the constant phase element (CPE) having relation with $C = (Q \cdot R)^{1/n} / R$ and $Q \approx C$ as $n \geq 0.9$) equivalent circuit combination in high frequency region as in Fig. S11(below) to evaluate true capacitances. This capacitance is due to space charge region at the copper oxide|electrolyte interface and capacitances at different bias voltage are used to construct the Mott-Schottky plot shown in Fig. 7a in the main text. The Mott-Schottky relation was used to work out V_{fb} and intrinsic carrier density (N_x , where $x = d$ for n-type and a for p-type). The values determined in this way, for desired RT-grown samples, are included in the Table 1(see main text) along with other properties as a function of O_{2pp} . The flatband potential converted to vacuum scale using similar method describe in the literature [4] and also depicted in Fig. 7 (main text) to identify conduction band (CB) and valence band (VB) with a common reference.

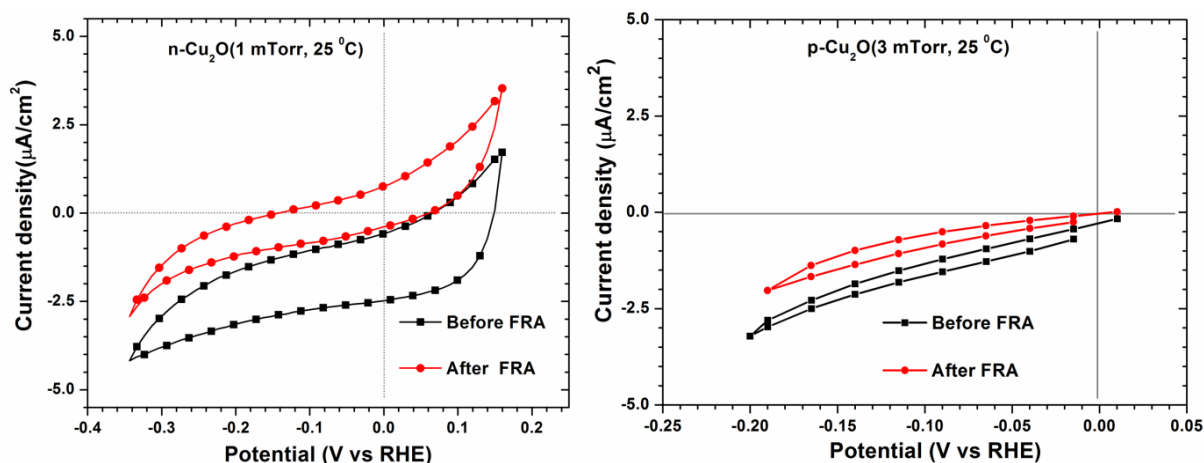


Fig. S10. Cyclic voltammograms of n- Cu₂O/ITO (left) and p-type Cu₂O/ITO (right) electrodes taken before and after frequency response analyses confirm that there was no-faradic process occurred during EIS measurement.

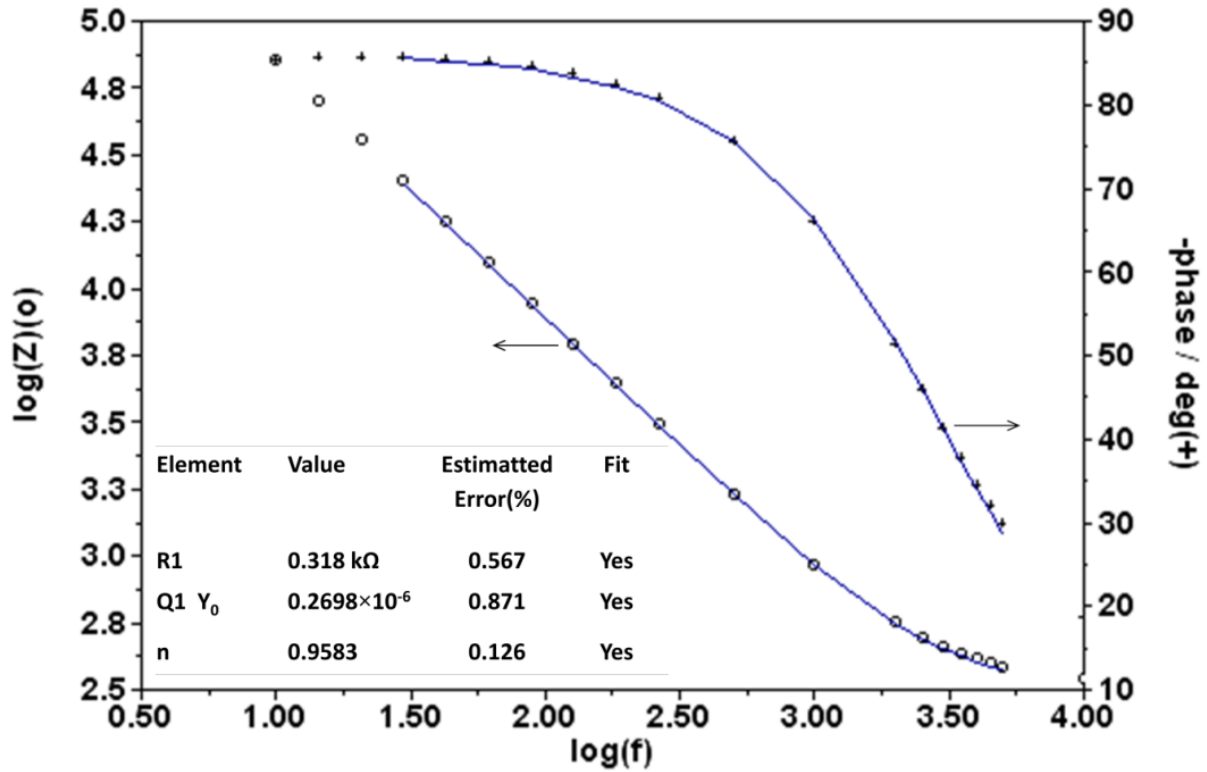


Fig. S11. Bode plot of EIS measurements of a RT-grown Cu₂O film on ITO in argon saturated 0.1M CH₃COONa electrolyte at -0.1 V vs RHE, the solid line represent the fits using an RQ equivalent(Q≈ C as n≥0.9). First few data points are eliminated to minimize the error in the best fitted impedance parameters (see inset table).

Calculation of effective density of states ($D(E_f)$) from EIS data:

The total double-layer capacitance (C_T) of copper oxide|electrolyte system can be calculated from the imaginary impedance (Z_{imag}) using equation [5]:

$$C_T = -1/(2\pi f Z_{imag}) \quad (S2)$$

where, f is the frequency. The space charge capacitance (C_{sc}) and Helmholtz capacitance (C_H)[6] can be related to C_T by following equation:

$$1/C_T = 1/C_{sc} + 1/C_H \quad (S3)$$

For, $\text{Cu}_2\text{O}/\text{ITO}$ electrode grown at 25°C with $\text{O}_{2pp} = 3 \text{ mTorr}$, using equation (S2) we got, $C_T = 11.25 \mu\text{F}/\text{cm}^2$ (where, $f = 29.76 \text{ Hz}$ and $-Z_{imag} \approx 6790 \text{ Ohm}$) at -0.21 V vs $\text{Ag}/\text{AgCl}(\approx 0 \text{ V}$ vs RHE) considering similar approach described in ref. [5].

Assuming $C_H \gg C_{sc}$; $C_{sc} \approx C_T \approx 11.25 \times 10^{-2} \text{ F}/\text{m}^2$

Therefore, the effective density states, $D(E_f) = (C_{sc})^2 / [\epsilon_0 \epsilon \cdot e^2] \approx 1.35 \times 10^{21} \text{ cm}^{-3}/(\text{eV})$.

[Or, incase of highly doped electrodes, assuming $C_H = 20 \mu\text{F}/\text{cm}^2$ [5] equation (S3) yields, $C_{sc} \approx 25.70 \mu\text{F}/\text{cm}^2$; $D(E_f) \approx 7.06 \times 10^{21} \text{ cm}^{-3}/(\text{eV})$]

where, ϵ_0 is permittivity of free space ($8.854 \times 10^{-12} \text{ F}\cdot\text{m}^{-1}$), ϵ is the relative dielectric constant (~ 6.6 for Cu_2O [7]) and e is the electronic charge $\sim 1.60 \times 10^{-19} \text{ C}$.

Similarly, we estimated effective density of states for other samples.

Fabrication of solid p-n junctions using p- and n-type Cu_2O :

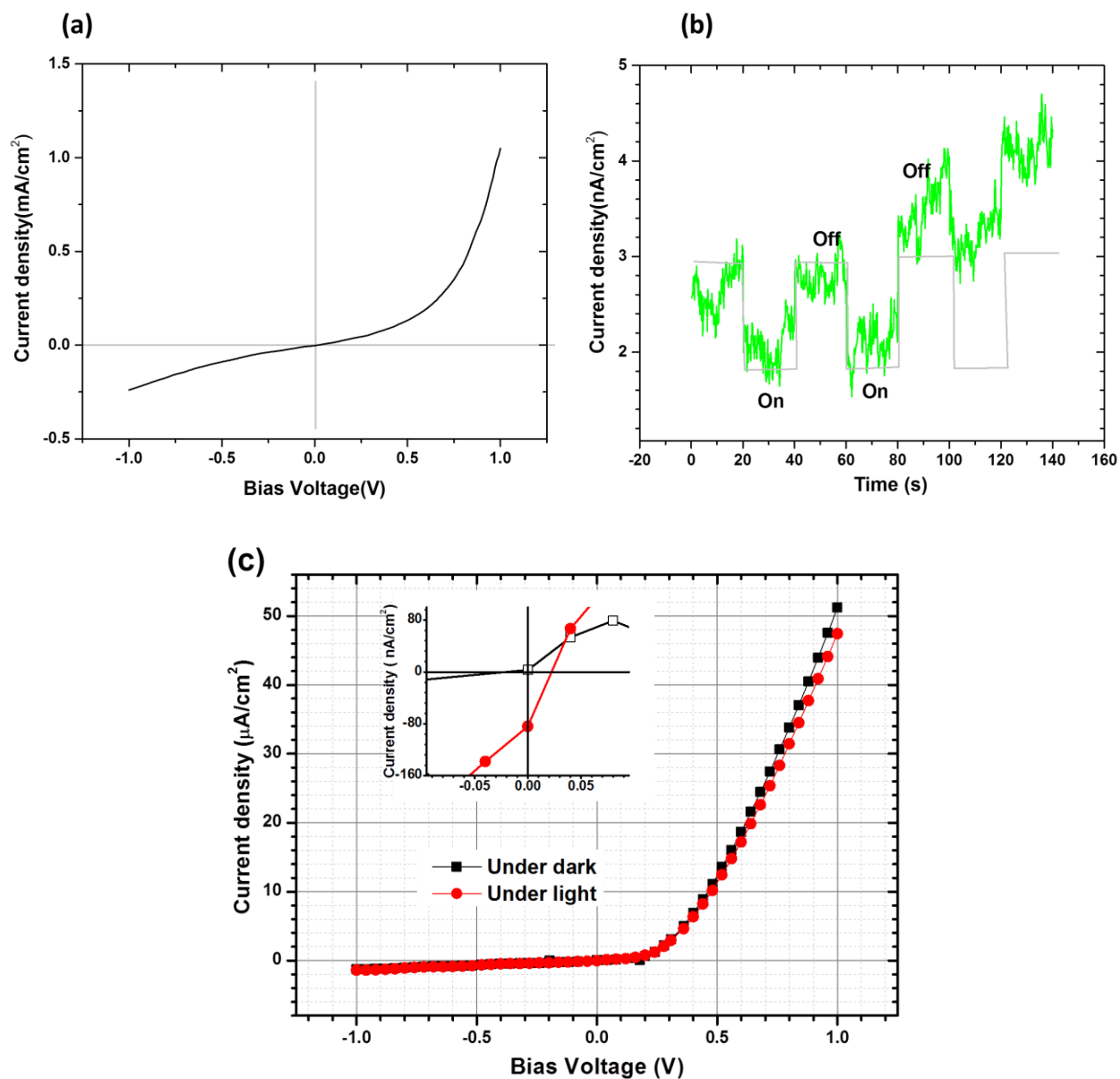


Fig. S12. The characteristic J-V curve for n-ZnO/p- Cu_2O (a, b) and n- Cu_2O /p-Si(111) (c) solar cells. Transient photocurrent of n-ZnO/p- Cu_2O cell measured under periodic LED illumination where 'On' and 'Off' step of the transient photocurrent (b) is demonstrated by the faint curve to assist the reader. A zoomed J-V curve under dark and light is shown in the inset of (c).

In Fig. S12a, the dark J-V characteristics curve of FTO/n-ZnO/p- Cu_2O /Au (cell#1) cell exhibited stable rectifying behaviour suggesting that a p-n junction was formed in the Cu_2O -ZnO system.

If p-n junction did not form, the dark and illuminated J-V curve would exhibit an ohmic behaviour and change the resistance of the system. The presence of high reverse saturation current of this cell is chiefly due to poor quality p-n junction (see Fig. S13 below). The downward shift of illuminated J-V curve was not consistent all time, therefore, taking an illuminated J-V curve within the narrow scanning range (e.g., -0.002 to +0.002V) would not produce reliable short circuit current (J_{sc}) and open circuit voltage (V_{oc}). However, the dynamic photo response at zero bias voltage of the same cell switching with the LED (wavelength just above the band gap of the absorber Cu_2O ($E_g \approx 2.2\text{eV}$ (564nm)) layer) by a pulse width of 20 sec exhibited very low and noisy photocurrent yet distinguishable from the dark current (see Fig. S12b). The synchronized ‘on’ and ‘off’ photo response of the cell#1 with the LED switching confirms that J_{sc} ($\sim 1 \text{ nA/cm}^2$) is real despite the noise fluctuation (see faint and green curve in figure S12b). Therefore, very low J_{sc} of the PV cell#1 could be attributed to low numbers of photogenerated charge carriers owing to ‘thin and poor quality’ Cu_2O layer ($\sim 53 \text{ nm}$) and thin ZnO ($\sim 114\text{nm}$) layer including an amorphous interfacial layer evident from the subsequent focused ion beam (FIB) cross-section and TEM analyses (see Fig. S13 below). Referring to Fig. S12b, the dark current density is increasing over time but the amplitude of the J_{sc} is remaining roughly the same on average ($J_{sc} \sim 1 \text{ nA/cm}^2$). The increase of dark current over time and low photocurrent might be attributed to the poor quality Cu_2O/ZnO junction owing to the presence of interfacial states which can serve as a recombination centre for the photogenerated charge carriers.

Fig. 8c shows the J-V characteristics curve of p-Si(111)/n- Cu_2O (cell#2) under dark and light (The I-V curve for ohmic contact for this cell can be found in Fig. S14). A zoomed part of this J-V curve is included in the inset of Fig. 8c to distinguish low $J_{sc} \sim 80 \text{ nA/cm}^2$ and $V_{oc} \sim 3 \text{ mV}$. Though a feeble PV performance, the J_{sc} and V_{oc} of cell#2 composed of PLD grown n-type Cu_2O on commercial p-Si substrate clearly better than cell#1. The interfacial investigation of cell#2 by FIB-TEM techniques was not done in this study which would give valuable information for further PV performance improvement.

Interface of n-ZnO/p-Cu₂O (cell#1):

To investigate the interface between ZnO and Cu₂O layer, a cross-section of the n-ZnO/p-Cu₂O(cell#1) cell was made by focused ion beam (FIB) technique. The SEM micrograph of the FIB specimen confirmed the formation of very thin but continuous Cu₂O (~53 nm) and ZnO (~114 nm) layer across the specimen (see figure S12 (top panel) overleaf). However, the subsequent TEM bright field (BF) image of the FIB specimen revealed an amorphous layer between the Cu₂O and ZnO layer (see figure S12 (bottom panel #4 inset) overleaf). It was expected that 30 min deposition time would give ~300 nm thick Cu₂O films, but both SEM and TEM BF image revealed a thickness which is much lower than the expected thickness. One possible reason might be the ZnO coating of quartz window occurred during ZnO film deposition step. Therefore, most of the UV-radiation might be absorbed or/and allow less amount (and less energetic) of radiation to fall on the Cu₂O target. This should affect the quantity of ablated species from the target as well as subsequent Cu₂O formation on the substrate. This means that one could expect a thin and poor quality Cu₂O film on any substrate, which resulted in poor quality interface between the deposited film and the substrate. A good quality Cu₂O film having absorption cross-section $\sim 10^5 \text{ cm}^{-1}$ near the band edge suggest that at least ~100 nm thick layer is necessary for sufficient numbers of photons to be absorbed. Thicker layer is also desired to avoid short-circuiting between inter layers. Therefore, very low J_{sc} of the present PV cell could be attributed to low numbers of photogenerated charge carriers owing to ‘thin and poor quality’ Cu₂O layer.

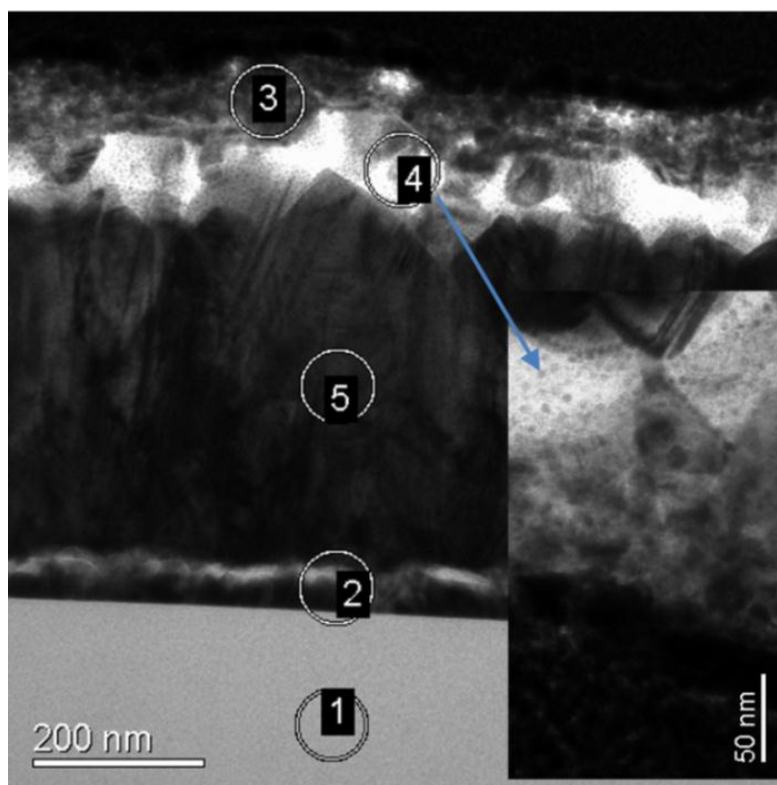
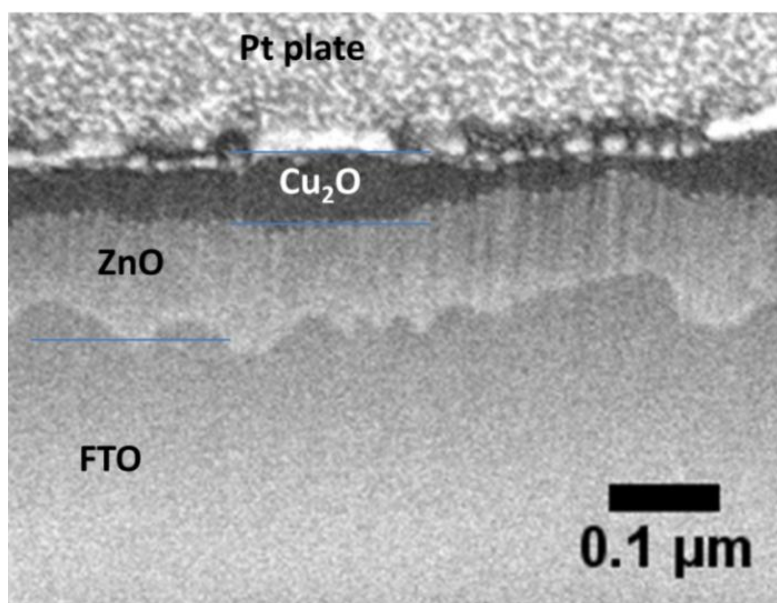


Fig. S13. FIB cross section of ZnO/Cu₂O solar cell junction (top): Cu₂O(~53nm), and ZnO(~114nm) layer. TEM Bright field image of the FIB cross-sectional sample (bottom left). Bottom left: Cu₂O(#3); amorphous layer(#4) between ZnO and Cu₂O layer(Shown bottom inset); FTO(#5) SiO₂(#2) and Glass(#1). Platinum (Pt)-plate was used to protect thin layers during FIB cross-sectional specimen preparation.

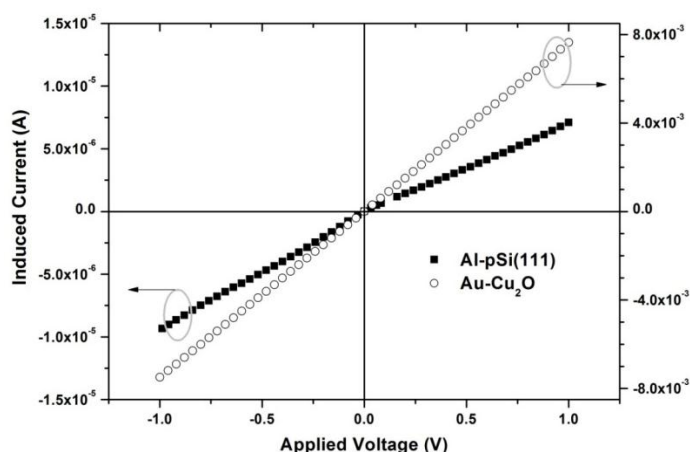


Fig. S14. I-V curve of p-Si (solid square) and n-Cu₂O (open circle) with aluminium and gold contacts showing ohmic behaviour.

References

- [1] S.F.U. Farhad, R.F. Webster, D. Cherns, Electron microscopy and diffraction studies of pulsed laser deposited cuprous oxide thin films grown at low substrate temperatures, *Materialia*, 3 (2018) 230 - 238.
<https://doi.org/10.1016/j.mtla.2018.08.032>
- [2] S.F.U. Farhad, Copper Oxide Thin Films grown by Pulsed Laser Deposition for Photovoltaic Applications, in: School of Physics, University of Bristol, UK, 2016, pp. 222.
<https://ethos.bl.uk/OrderDetails.do?uin=uk.bl.ethos.691178>
- [3] Van der Pauw Hall Measurement worksheet, Physical Measurement Laboratory, National Institute of Standards and Technology (NIST). Accessed on 27/05/2020. <https://www.nist.gov/pml/nanoscale-device-characterization-division/popular-links/hall-effect/sample-hall-worksheet>
- [4] C.M. McShane, K.S. Choi, Junction studies on electrochemically fabricated p-n Cu₂O homojunction solar cells for efficiency enhancement, *Physical chemistry chemical physics* : PCCP, 14 (2012) 6112-6118.
<https://doi.org/10.1039/C2CP40502D>
- [5] B. Bera, A. Chakraborty, T. Kar, P. Leuaa, M. Neergat, Density of States, Carrier Concentration, and Flat Band Potential Derived from Electrochemical Impedance Measurements of N-Doped Carbon and Their Influence on Electrocatalysis of Oxygen Reduction Reaction, *The Journal of Physical Chemistry C*, 121 (2017) 20850-20856.
<https://doi.org/10.1021/acs.jpcc.7b06735>
- [6] K. Uosaki and Hideaki Kita, Effects of the Helmholtz Layer Capacitance on the Potential Distribution at semiconductor/Electrolyte Interface and the Linearity of the Mott-Schottky Plot, *Journal of The Electrochemical Society*, 130 (1983) 895. <https://doi.org/10.1149/1.2119853>
- [7] A. Paracchino, J.C. Brauer, J.-E. Moser, E. Thimsen, M. Graetzel, Synthesis and Characterization of High-Photoactivity Electrodeposited Cu₂O Solar Absorber by Photoelectrochemistry and Ultrafast Spectroscopy, *The Journal of Physical Chemistry C*, 116 (2012) 7341-7350. <https://doi.org/10.1021/jp301176y>